SEDIMENTOLOGY the journal of the International Association of Sedimentologists IAS

Sedimentology (2024) **71**, 1843–1872 doi: 10.1111/sed.13194

The latest Jurassic–earliest Cretaceous climate and oceanographic changes in the Western Tethys: The Transdanubian Range (Hungary) perspective

DAMIAN G. LODOWSKI*,† , OTTILIA SZIVES‡ , ATTILA VIRÁG§,¶ and JACEK GRABOWSKI*

*Polish Geological Institute – National Research Institute, ul. Rakowiecka 4, Warsaw 00-975, Poland (E-mail: damian.lodowski@uw.edu.pl; damian.lodowski@pgi.gov.pl)

†Faculty of Geology, University of Warsaw, ul. Żwirki i Wigury 93, Warsaw 02-089, Poland

‡Department of Collections, Geological Survey, Supervisory Authority for Regulatory Affairs, Stefánia út 14, Budapest 1143, Hungary

§Department of Petrology and Geochemistry, Institute of Geography and Earth Sciences, Eötvös Loránd University, 1/c Pázmány Péter sétány, Budapest H-1117, Hungary (E-mail: attila.virag@ttk.elte.hu)

¶Department of Mineralogy and Geology, Institute of Earth Sciences, University of Debrecen, 1 Egyetem tér, Debrecen H-4032, Hungary

Associate Editor – J.P. Walsh

ABSTRACT

The Jurassic/Cretaceous transition was characterized by several distinct palaeoenvironmental processes and events, amongst which some of the best known are the late Tithonian–early Berriasian aridization and the late Berriasian tectonic reactivation in the Neotethyan Collision Belt. This study aims to reconstruct the latest Jurassic–earliest Cretaceous palaeoenvironment and its evolution in the area of the Transdanubian Range (Hárskút and Lókút successions, Hungary), and provide new data on the relation between climate changes, palaeoceanography and marine ecosystems. Herein, calcareous nannofossil and geochemical data are presented and put into a geochronological framework in order to evaluate and compare palaeoenvironmental signals recorded in the two studied successions; the resultant scenario is compared with published literature data from both the western Tethyan region and northern Europe. Accordingly, in the Transdanubian Range, the relatively humid climate of the early Tithonian was followed by the late Tithonian–early Berriasian arid phase and the late Berriasian humidification. Besides, two intervals of palaeoceanographic perturbations were documented in the upper Tithonian–lowermost Berriasian (OD I), and the lower/upper Berriasian transition beds (OD II); these are manifested by the record of seafloor hypoxia and elevated accumulations of micronutrients, as well as changes in calcareous nannofossil assemblages. In the view of this study, the most probable trigger of the late Tithonian–early Berriasian aridization was a restriction in the atmospheric circulation (including monsoons), which was forced by climate cooling and lowering thermal gradient between landmasses and the ocean. Under such conditions, the mechanism of a wind-induced water mixing might become less efficient, driving seawater stratification, seafloor hypoxia and increased burial of nutrients. Although the humid climate of the late Berriasian likely resumed the monsoon-type circulation, the

[Correction added on 29 April 2024, after first online publication: Attila Virág was designated as corresponding author].

tectonic reactivation and uplift in the NeoTethyan Collision Belt might have effectively separated the Bakony Basin from the 'open' NeoTethys, which hampered the marine circulation and efficient water mixing in the former.

Keywords Berriasian, calcareous nannofossils, geochemistry, palaeoenvironment, pelagic successions, Tithonian, Transdanubian Range, western Tethys.

INTRODUCTION

The Jurassic/Cretaceous (J/K) transition was a time of multiple important environmental changes, which manifest both in lithological appearance (i.e. switch from the siliceous to carbonate deposition, or the later disappearance of the *Ammonitico Rosso* facies; e.g. Cecca *et al.*, 1992; Jach & Reháková, 2019), and numerous palaeoecological perturbations (i.e. series of calcareous nannofossil evolutionary events, displacement of radiolarians by calpionellids, or the disappearance of planktonic crinoids of the genus *Saccocoma*; Casellato, 2009; Grabowski *et al.*, 2019; Jach & Reháková, 2019; Casellato & Erba, 2021; Lodowski *et al.*, 2022). Those phenomena are considered as resulting from different factors controlling the marine ecosystem, amongst which the most important are: (i) bioproductivity, which is predominantly conditioned by the availability of nutrients within the photic zone; (ii) seafloor oxygenation, which has an impact on the benthic fauna on one hand and inform about the intensity of marine circulation (mixing of the water column) on the other; and (iii) water pH, which affects the amount of available CO_3^{2-} ions for biocenosis (i.e. Weissert & Mohr, 1996; Weissert *et al.*, 1998; Weissert & Erba, 2004). The abovementioned parameters were additionally modified and/or controlled by other, higher-rank (and often overlapping) environmental processes, such as climate changes, eustasy and tectonic activity.

Recently, accumulation of nutrient-type elements in carbonates was associated with activity and the strength of monsoonal upwellings by Lodowski & Grabowski (2023). De Wever *et al.* (2014) came to the conclusion that the widely opened Tethys Ocean during the Mesozoic was favourable for strong monsoons, which might effectively trigger upwelling currents, sea-surface nutrition and widespread deposition of radiolarites (see also Baumgartner *et al.*, 2023). In turn, Baumgartner (2013) considered that radiolarian blooms were driven by riverine supply of nutrients. Nonetheless, it still remains unclear which of the abovementioned models describes the actual process, or to what extent they interplayed in different sedimentary zones.

One of the areas possessing a great potential for such considerations is the Transdanubian Range (Hungary). During the latest Jurassic–earliest Cretaceous, it was located far from neighbouring lands, which ensured almost complete deprivation of external factors (such as high continental runoff) recording of sedimentary trends and events. Besides, variegated seafloor palaeotopography (Vörös & Galácz, 1998) allows to evaluate and compare how (and to what extent) different environmental changes manifest in different palaeobathymetric zones of the single sedimentary basin. This study examines calcareous nannofossil assemblages and various climate-related, redox-related and productivity-related geochemical proxies. The resultant scenario was compared with published data concerning both the Western Tethyan and Subboreal domains; combined, this information enabled preparation of a concise palaeoenvironmental model. This may significantly contribute not only to understanding of the latest Jurassic–earliest Cretaceous environmental changes in the Western Tethys, but also in other geographic domains and during different epochs.

GEOLOGICAL SETTING

Geological framework of the Transdanubian Range

The Mesozoic cover of the Transdanubian Range (TR) accounts for the record of the sedimentary zone in between the Neotethys Ocean to the south-east and the Alpine Atlantic to the north-west (Haas & Péró, 2004; Szederkényi *et al.*, 2013; Fig. 1). Since the Early Jurassic, the sedimentation in the TR was periodically affected by the subduction in western parts of the Neotethys Ocean, and related formation of the 'Neotethyan Collision Belt' (NCB; Kozur, 1991; Missoni & Gawlick, 2010). During the Late Jurassic, the area of the TR was characterized by a 'horst and graben' type of deposition, this however gradually became

more flattened in the earliest Cretaceous (Vörös & Galácz, 1998; see also Szederkényi *et al.*, 2013). In the context of this study, also of considerable importance was the late Berriasian tectonic reactivation in the NCB (Császár & Árgyelán, 1994; Árgyelán, 1997).

This research involves the data collected from the uppermost Jurassic–lowermost Cretaceous strata of the Hárskút and Lókút successions. They record different palaeobathymetric zones, with the Hárskút composite section (HK-12 and HK-12/a) being deposited on a submarine elevation and the Lókút sections (LO-I and LO-II) recording a more basinal setting of the Bakony Basin (Fig. 1). The sedimentary succession consists of Oxfordian radiolarites, Kimmeridgian–(cf.)

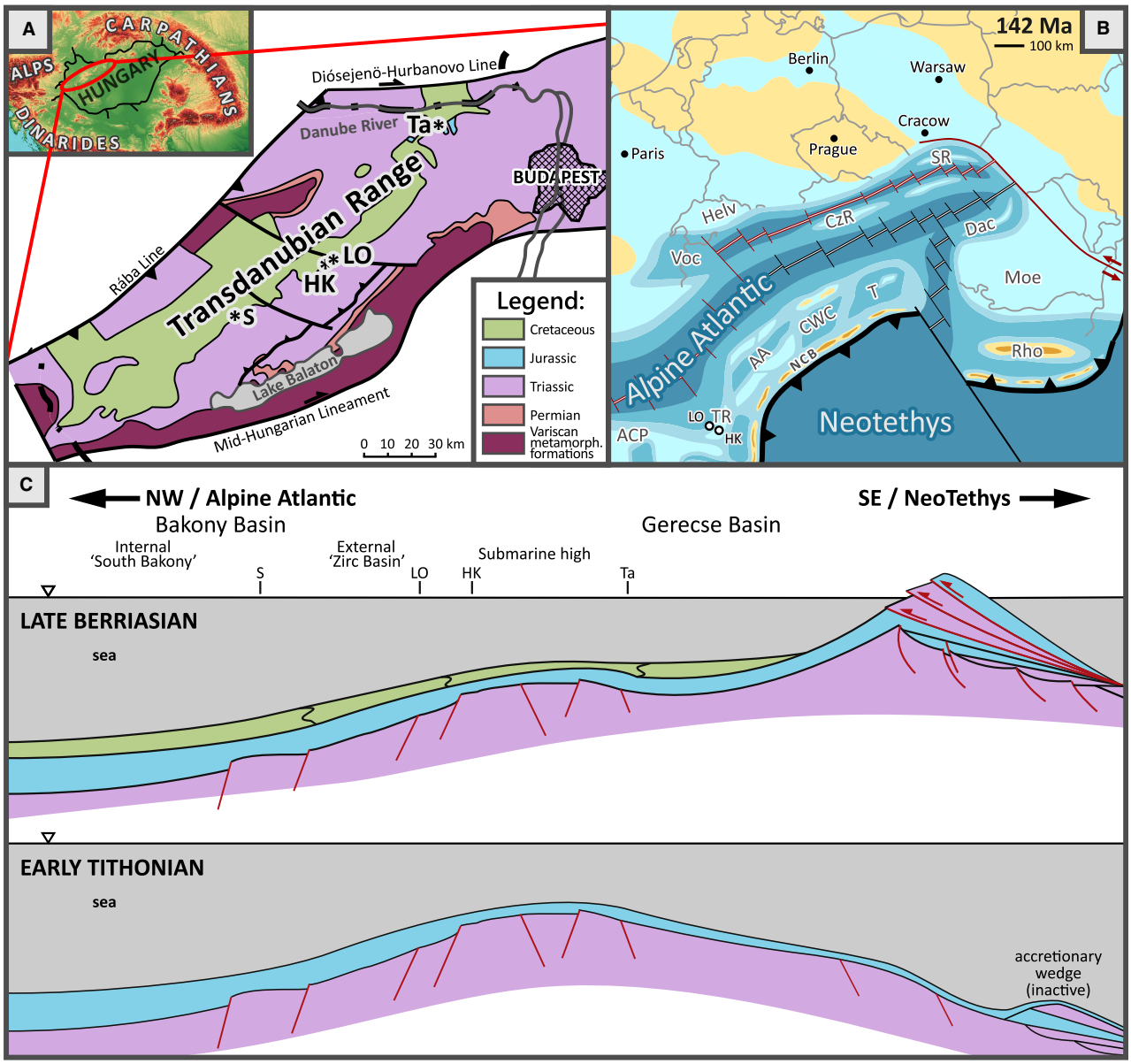

Fig. 1. Geological setting of the study area. (A) Simplified pre-Cenozoic map of the Transdanubian Range Unit, as in Lodowski *et al.* (2022). (B) Simplified palaeogeographical map of the circum Carpathian region during the early Berriasian. (C) Conceptual reconstruction of the latest Jurassic–earliest Cretaceous structure of the Transdanubian Range (modified after Grabowski *et al.*, 2017). Abbreviations: LO – Lókút; HK – Hárskút; S – Sümeg; Ta – Tata; T – Tisia; AA – Austro Alpine; ACP – Adriatic Carbonate Platform; CWC – Central Western Carpathians; DAC – Dacia; NCB – Neotethyan Collision Belt; CzR – Czorsztyn Ridge; Helv – Helvetic units; Moe – Moesian Platform; Rho – Rhodopes; SR – Silesian Ridge; TR – Transdanubian Range; Voc – Vocontian Basin.

mid-Tithonian *Ammonitico Rosso*-type limestones and the upper Tithonian–lower Valanginian *Biancone*/*Maiolica* facies; characteristic of the Hárskút sections is also one of the youngest so-far known appearances of the red nodular limestone, late Berriasian–earliest Valanginian in age. In recent years a detailed biostratigraphic, chemostratigraphic and magnetostratigraphic framework of the Hárskút and Lókút sections was established by Főzy *et al.* (2010), Grabowski *et al.* (2010, 2017), Price *et al.* (2016), Lodowski *et al.* (2022) and Szives & Főzy (2022) (Fig. 2). The most characteristic sedimentary features of the Hárskút and the Lókút successions are visualized in Appendix S1.

Palaeoclimate context

The J/K transition was marked by a well-pronounced arid phase, which is best documented from the Tithonian–lowermost Berriasian sequences of northern Europe, where extensive data on clay minerals (i.e. Deconinck *et al.*, 1983; Wignall & Ruffel, 1990; Hallam *et al.*, 1991; Hesselbo *et al.*, 2009; Błażejowski *et al.*, 2023), K-based proxies (Schnyder *et al.*, 2006; Hesselbo *et al.*, 2009; Grabowski *et al.*, 2021a; Błażejowski *et al.*, 2023) and palynology (Abbink *et al.*, 2001; Schneider *et al.*, 2018) are available. Related phenomena of the late Tithonian climate aridization and/or the late Berriasian humidification were reported also from the Jura Mountains (Rameil, 2005; Bover-Arnal & Strasser, 2013), Vocontian Basin (Deconinck, 1993; Morales *et al.*, 2013), central Tunisia (Schnyder *et al.*, 2005), and the Central Western Carpathians (Lodowski & Grabowski, 2023) and Balkan area (Grabowski *et al.*, 2021b). Several authors also provided some arguments on the occurrence of a so-called 'cold snap' event (relatively short lasting cooling; even glaciation) during the latest Jurassic (and possibly earliest Cretaceous); nonetheless, its scope and amplitude is not well-constrained yet (e.g. Gröcke *et al.*, 2003; Weissert & Erba, 2004; Tremolada *et al.*, 2006; Jenkyns *et al.*, 2012; Schneider *et al.*, 2020; Baumgartner *et al.*, 2023).

MATERIALS AND METHODS

Calcareous nannofossils

Due to the fact that changes in composition and diversity of calcareous nannofossil assemblages may relate to palaeoecological changes, this paper considers their total abundance (TA) and relative abundance (RA), as well as Fischer alpha (diversity) index (Fisher *et al.*, 1943; Giraud *et al.*, 1998; Pittet & Mattioli, 2002).

A total of 95 samples (39 from the lower Berriasian of the Lókút LO-I, and 71 from Hárskút HK-12 and HK12/a sections) were investigated, adopting a simple smear slide preparation method (Bown & Young, 1998). This technique does not guarantee the homogeneity of the material, therefore the mean particle density of each smear slide was calculated based on 12 random views at 40× magnification. Percentage of the material on each slide was estimated using the Bacelle & Bosselini (1965) plates. Nannofossils were counted under the Nikon Eclipse 50i POL polarizing microscope (Nikon, Tokyo, Japan), using oil immersion objective ×100 and a 1.25 numerical aperture. For each slide a 60×60 field of view (FOV) matrix was adopted, which accounts for the uniform number of 3600 FOVs.

A descriptive statistical analysis (Pearson Correlation Coefficients, PCC's) was performed using the R-software, examining only those samples in which: (i) counts per slide exceed 125 (TA >0.35); (ii) RA of *Watznaueria barnesiae* is below 70%; and (iii) taking into account only those taxa which account for more than 1% of the population in average (see Pittet & Mattioli, 2002). Due to the large number of samples with less than 300 counts, PCA/DCA methods were not applied. The taxonomy follows the Nannotax website (Young *et al.*, 2017).

A numerical matrix of investigated assemblages is attached in Appendix S2 Excel® file; the R-software script is provided as Appendix S3. All of the smear slides were prepared, investigated and are reposited in the Department of Collections, Geological Survey, Supervisory Authority for Regulatory Affairs, Budapest. This study incorporates also the data of Stoykova (Grabowski *et al.*, 2017), collected in the Lókút succession.

Elemental geochemistry

Chemical analyses of 86 whole-rock samples were performed at the Bureau Veritas Minerals Laboratories, Canada, using the multi-acid MA250 method (for details see Bureau Veritas Minerals Schedule of Service & Fees, 2020). For the Tithonian–lowermost Berriasian of the Lókút succession this study adopts the data of Grabowski *et al.* (2017).

Different palaeoclimate processes are examined herein using the following geochemical proxies: (i) Zr/Al, to estimate the energy and relative

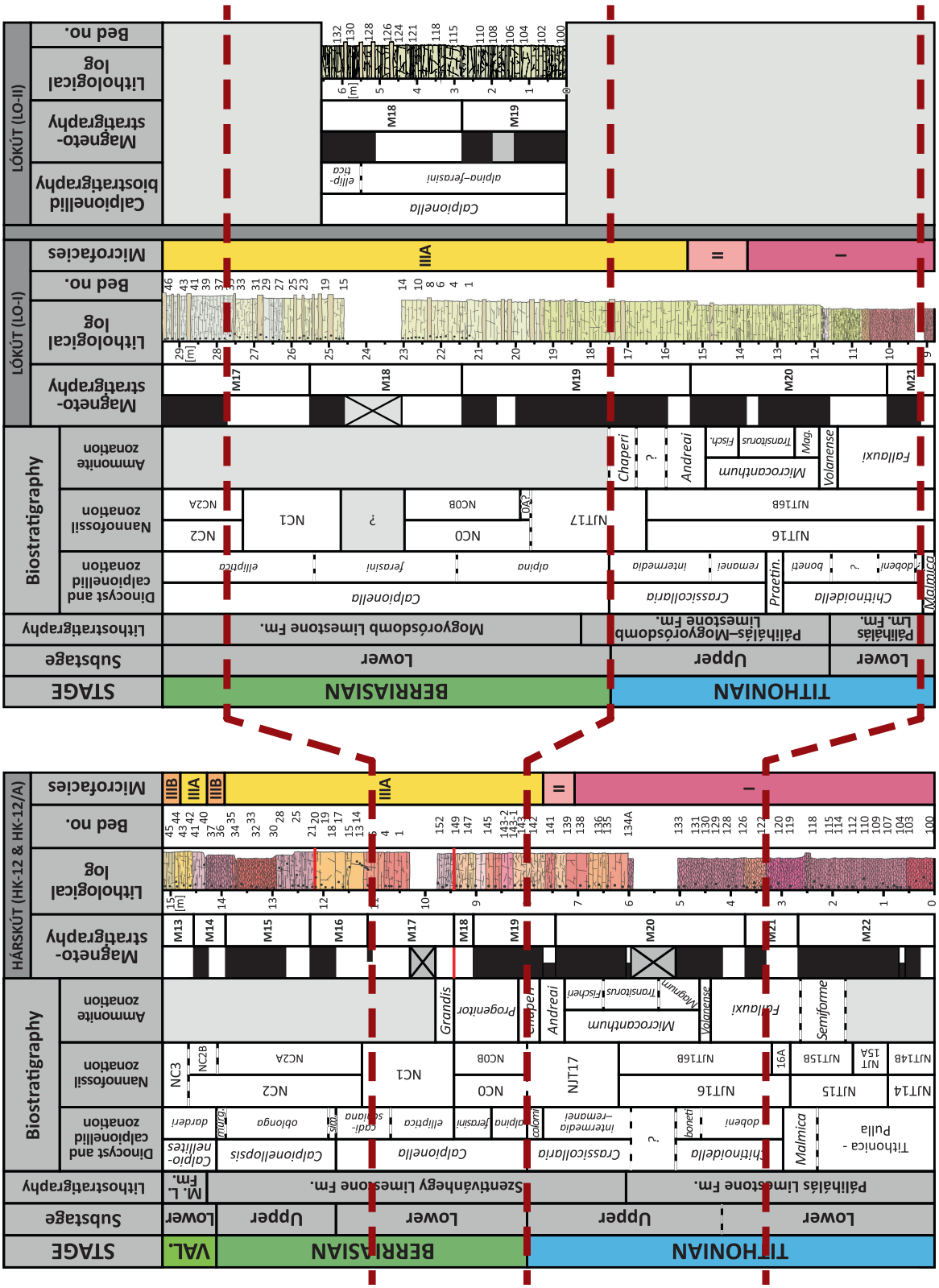

Fig. 2. Stratigraphic framework and correlation of the Hárskút (left) and Lókút (right) successions (after Lodowski *et al.*, 2022). Abbreviations: VAL. – Valanginian; murg. – Murgeanui; sim. – simplex; Mag. – Magnum; Fisch. – Fischeri; Praetin. – Praetintinnopsella. MF I – *Saccocoma*-dominated microfacies; MF II – transitional microfacies; MF IIIA – calpionellid wackstone/packstone; MF IIIB – bioclastic wackestone/packstone.

contribution of the aeolian fraction (e.g. Schnetger *et al.*, 2000; Calvert & Pedersen, 2007); (ii) Ga/Rb, which is a proxy of kaolinite/illite proportions, given that Al is easily substituted by Ga in kaolinite (Hieronymus *et al.*, 2001), while Rb readily replaces K in the illite structure (see also Ratcliffe *et al.*, 2010; Grabowski *et al.*, 2021a); (iii) Chemical Index of Alteration (CIA), to approximate the strength of chemical weathering on continents (Nesbitt & Young, 1982); as well as (iv) Th/K (Schnyder *et al.*, 2006), Ti/K (Grabowski *et al.*, 2021a,b) and Al/K (Wei *et al.*, 2006), to collect data on climate related leaching of potassium. The CIA was calculated adopting the formula of Nesbitt & Young (1982):

$$\mathrm{CIA} = \left[\frac{\mathrm{Al_2O_3}}{\mathrm{Al_2O_3} + \mathrm{CaO^*} + \mathrm{Na_2O} + \mathrm{K_2O}}\right] \times 100\%$$

where CaO* is the amount of CaO incorporated in the silicate fraction of the rock. Elemental concentrations of given elements were stoichiometrically converted to their oxide equivalents, whereas silicate CaO is approximated to the proportion of Na_2O (i.e. McLennan, 1993).

To investigate whether sediments were subjected to oxygen depletion, uranium concentrations have been recalculated with respect to the authigenic *U* formula of Jones & Manning (1994):

$$\text{Authigenic } U = U_{\mathrm{SAMPLE}} - \left(\frac{\mathrm{Th_{SAMPLE}}}{3}\right)$$

To evaluate the palaeoredox signal recorded in Mo (e.g. Algeo & Li, 2020; Algeo & Liu, 2020) its enrichment factors (EF) were calculated, following the formula of Li & Schoonmaker (2003):

$$\mathrm{EF}_X = \frac{\frac{X_{\mathrm{SAMPLE}}}{\mathrm{Al_{SAMPLE}}}}{\frac{X_{\mathrm{AVERAGE\ SHALE}}}{\mathrm{Al_{AVERAGE\ SHALE}}}}$$

where *X* is the element considered. Ultimately, also U/Th (Jones & Manning, 1994) and Fe/Al (Algeo & Liu, 2020) ratios were examined.

Bioproductivity-related processes are considered herein based on those elements which are known for their importance for biological processes (P, Zn and Cu) and/or are characterized by nutrient-like distribution in sediments (Ba) (Tribovillard *et al.*, 2006). Here are examined their enrichment factors (see above), biological ('excess') concentrations and accumulation rates (AR) of 'excess' fraction. Biological fluxes were approximated using the equation of Shen *et al.* (2015):

$$X_{\mathrm{EXCESS}} = X_{\mathrm{SAMPLE}} - (\mathrm{Al_{SAMPLE}} \times D)$$

where *X* is the examined element while *D* is a 'detrital' constant, approximated as the lowest non-protruding *X*/Al ratio in the entire dataset (see also Rutsch *et al.*, 1995; Grabowski *et al.*, 2021b). The AR's were calculated using the formula:

$$X_{\mathrm{AR}} = X(\mathrm{mg/g}) \times \text{rate of deposition}(\mathrm{cm/kyr}) \times d(\mathrm{g/cm^3})$$

where *X* is the 'excess' content of examined element and *d* is rock density (see Schoepfer *et al.*, 2015; Shen *et al.*, 2015). Sedimentation rates were taken from Lodowski *et al.* (2022), whereas rock density was arbitrarily set to 2.5 g/cm^3, following the average densities of palaeomagnetic samples examined by Lodowski *et al.* (op. cit.). All of the geochemical data examined during this study are available in a numerical form in the Appendix S2 Excel® file.

RESULTS

Calcareous nannofossils

Diagenesis and preservation

According to classification of Roth (1984), nannofossil assemblages of the Hárskút and Lókút successions are poorly to moderately preserved. Total abundance (TA) values are extremely low, while specimens display etching and dissolution features, suggestive of possible diagenetic alteration. In order to evaluate whether nannofossils were affected by diagenesis, RA of *Watznaueria barnesiae* was plotted against richness (number of species; see Erba *et al.*, 1992). When considering all samples, scatter plots reveal a negative correlation ($r = -0.44$) between richness and RA of *W. barnesiae* (Fig. 3). When examining only those samples in which *W. barnesiae* account for less than 70% of the assemblage, correlation decreases only slightly ($r = -0.4$), indicative of rather limited (or no) post-depositional effects. Also in Hárskút sections RA of *W. barnesiae* usually does not exceed 70%, whereas weak correlation between the taxa and richness ($r < 0.5$ in samples with *W. barnesiae* below 70%; Fig. 3) indicate no diagenetic bias.

Nannofossil assemblage composition

The RA values of five groups are visualized on Fig. 4: (i) small *Cyclagelosphaera* spp. (mostly *C.*

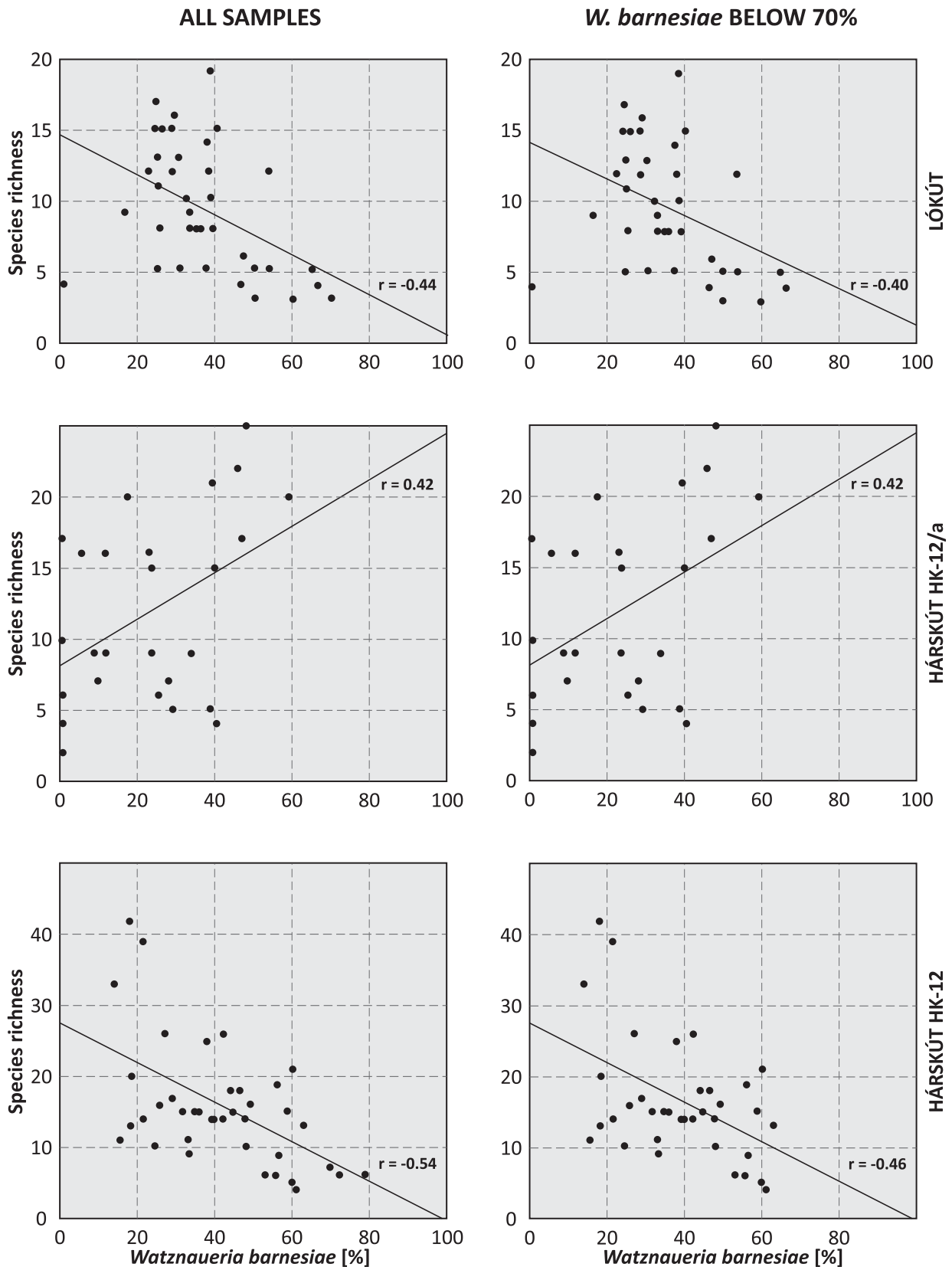

Fig. 3. Scatter plots of relative abundances of *Watznaueria barnesiae* versus species richness in Lókút and Hárskút sections. Left charts: all samples; right charts – samples in which RA *W. barnesiae* does not exceed 70%.

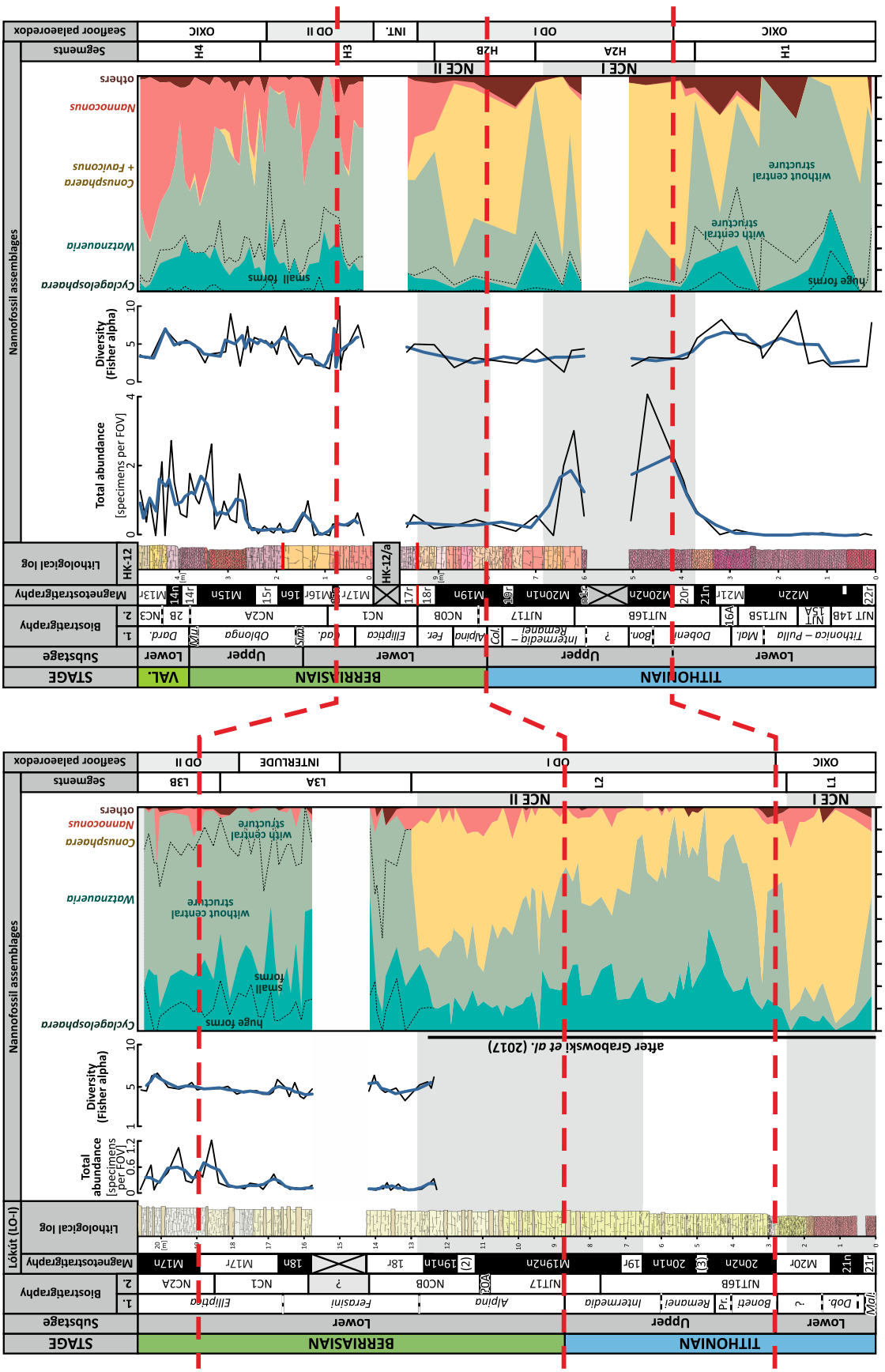

Fig. 4. Total abundances (TA), Fischer alpha (diversity index) and vertical relative abundances (RA) of selected key groups of the Tithonian–Berriasian calcareous nannofossils in the Lókút (left) and Hárskút (right) successions. Blue lines represent three-point moving averages. Data for the Tithonian–lowermost Berriasian of the Lókút succession after Grabowski *et al.* (2017).

margerelii) and huge *Cyclagelosphaera* spp. (*C. brezae*, *C. deflandrei* and *C. argoensis*), separately (following Giraud *et al.*, 2016); (ii) *Watznaueria* spp. (taxa with and without central structure separately); (iii) *Conusphaera* + *Faviconus* spp.; (iv) *Nannoconus* spp.; and (v) other taxa.

The TA per FOV are – typically for smear slides prepared from limestones – very low (0 to 4) in both successions studied (Fig. 4) and are generally lower in Lókút. In order to investigate whether low TA's reflect the original scarcity of the nannofossil assemblages, occasional thick smear slides were prepared; these confirmed the lower TA of nannofossils in the Lókút succession. On average, 22 nannofossils per slide (up to 868 specimens) occur in the Lókút samples, whereas the mean of 24 specimens account for the Hárskút composite section (up to 1608). Three barren samples come from the lower Berriasian of the Lókút, whereas another nine were identified in the Hárskút sections.

Lókút succession

The lower Berriasian of the Lókút succession displays low and generally parallel TA and Fischer alpha; characteristic are also elevated TA's in the topmost M17r and M17n magnetozones (Fig. 4). Quantitative analyses revealed that eight groups (*W. barnesiae*, *Cyclagelosphaera margerelii*, *Watznaueria* cf. *cynthae*, *Watznaueria* sp., *Watznaueria biporta, Watznaueria fossacincta*, *Cyclagelosphaera brezae* and *Cyclagelosphaera argoensis*) display relative abundances exceeding 3% (Table 1).

The basal part of the succession (M21r–M20r) is dominated by *Conusphaera* spp.; above (M20n–M19n), after an initial expansion of *Watznaueria* spp. (cf. M20n), *Conusphaera* regains importance and becomes dominant again. For the upper part of the succession (M18r–M17n) characteristic is the lack of *Conusphaera* spp., which were replaced by *Watznaueria* spp. (mostly *W. barnesiae*, with a mean RA – 46.38%) and various taxa of *Cyclagelosphaera* as additional elements (Fig. 4).

Within the upper part of the Lókút succession (above M18r), *W. barnesiae* most frequently occurs together with *Cyclagelosphaera deflandrei* ($r = 0.85$), frequently with *C. margerelii* (PCC = 0.93) and less likely with *W. fossacincta* (−0.71). Besides, *C. margerelii* is unlikely to be observed together with *Watznaueria bayackii* (−0.86) and *W. fossacincta* (−0.82) (Table 2A). Although rare and below statistical significance, some proxy forms occur within the uppermost part of the succession: a single specimen of *R. asper* was found in bed LO33, and five specimens of *Z. embergeri* come from beds LO39, LO41 and LO43.5 (Appendix S2).

Hárskút succession

Except for the two distinctive peaks within the lower part of the upper Tithonian (magnetozone M20n2n and the basal part of M20n1n), TA's remain low and very low; diversity, in turn, is higher within the lower Tithonian beds and manifests a negative correlation with TA (Fig. 4). Calcareous nannofossil assemblage of the lower Tithonian is dominated by *Watznaueria* spp., which are replaced by *Conusphaera* spp. in the upper Tithonian–lowermost Berriasian. Within the lower Berriasian, *Conusphaera* almost absolutely disappears, being suppressed by *Watznaueria* and *Nannoconus* spp. Ultimately, the upper Berriasian–lower Valanginian is characterized by the rise and subsequent dominance of *Nannoconus* spp. (Fig. 4).

In the HK-12/a section (Tithonian–lowermost Berriasian) only four taxa exceed 3% of RA (*Conusphaera mexicana mexicana*, *W. barnesiae*, *Watznaueria manivitae* and *C. margerelii*). The most abundant is *C. mexicana mexicana*, with a mean of 31.1%, followed by *W. barnesiae* (23.5%) (Table 1). A very strong negative correlation is observed between *C. mexicana mexicana* and *W. barnesiae* (PCC = −0.98) (Table 2). In contrast, *Watznaueria biporta* displays a strong positive correlation with *Polycostella senaria* (= *Nannoconus erbae*, according to Varol & Bowman, 2019; $r = 0.88$), *W. fossacincta* (0.86), *Conusphaera mexicana minor* (0.86), *W. barnesiae* (0.84) and *C. margerelii* (0.84) (Table 2B).

The Berriasian part of the succession (HK-12 section) has five groups with RA ≥3%: *W. barnesiae*, *C. margerelii*, *Nannoconus steinmannii steinmannii*, *Nannoconus* narrow canal top view and *Nannoconus infans*; the most abundant is *W. barnesiae* with a mean of 39.5%. Correlation between various taxa is not well-expressed; only *Watznaueria ovata* occur quite often with *W. biporta* (0.64), whilst *W barnesiae* shows a negative load to *N. steinmannii steinmannii* (−0.77). Ultimately, a slight positive load (0.41) is observed between *W. barnesiae* and *C. mexicana mexicana*, which contrasts with their strong negative phase in the HK-12/a section. Amongst proxy forms, HK-12 section contains rare specimens of *R. asper* (HK26 and HK36 beds) and *Z. embergeri*, which systematically appear above bed HK26 (Appendix S2).

Table 1. Descriptive statistics of selected taxa (mean ≥1%) from the Lókút and Hárskút successions. Min. – minimum; Max. – maximum; SD – standard deviation; SE – standard error; SK – skewness; KS – kurtosis.

Species	Mean [%]	Median [%]	Min. [%]	Max. [%]	SD	SE	SK	KS
Lókút succession								
LO-I								
W. barnesiae	36.38	35.25	0	66.67	13.60	2.21	0.15	3.42
C. margerelii	17.77	15.67	0	46.15	10.56	1.71	0.92	3.54
W. cf. *cynthae*	7.38	6.87	0	25.00	7.06	1.14	0.59	2.44
Watznaueria sp.	7.03	0	0	50.00	11.58	1.88	1.96	6.66
W. biporta	6.50	8.2	0	20.10	5.74	0.93	0.28	2.08
C. fossacincta	5.83	4.72	0	17.86	5.71	0.93	0.47	1.99
C. brezae	4.42	4.55	0	12.90	3.81	0.62	0.38	2.18
C. argoensis	3.76	2.97	0	15.89	3.70	0.60	1.11	4.27
C. deflandrei	2.18	0.87	0	20.00	3.90	0.63	3.04	13.2
W. britannica	1.98	0	0	16.67	3.53	0.57	2.58	9.91
Nannoconus spp. top view <10 μm	1.86	0	0	25.00	4.39	0.71	4.18	21.73
W. bayackii	1.77	0	0	25.00	4.68	0.76	3.75	17.80
Hárskút succession								
HK-12								
W. barnesiae	39.50	39.76	13.83	62.99	14.63	2.37	0.1	1.86
C. margerelii	13.37	13.19	1.43	27.78	6.17	1.00	0.24	2.89
N. steinmannii steinmannii	10.34	8.30	0	30.25	8.60	1.39	0.68	2.39
Nannoconus spp. top view <10 μm	5.53	4.90	0	28.04	5.86	0.95	1.63	6.88
N. infans	4.76	2.85	0	25.00	6.51	1.06	1.56	4.57
N. alvus	2.94	1.98	0	20.00	4.14	0.67	2.28	9.22
W. bayackii	2.9	2.32	0	13.04	3.14	0.51	1.39	4.87
W. biporta	1.67	0	0	17.31	3.53	0.57	2.97	12.25
N. magnadiscus	1.56	0.14	0	7.73	2.36	0.38	1.46	3.72
W. cf. *cynthae*	1.23	0	0	17.78	3.16	0.51	4.12	21.26
C. mexicana mexicana	1.18	0	0	12.82	2.63	0.43	3.05	12.54
N. bronnimannii	1.13	0	0	7.69	1.95	0.32	1.68	5.04
Nannoconus (small, flat)	1.12	0	0	7.69	1.78	0.29	1.83	6.25
W. britannica	1.12	0.56	0	7.41	1.62	0.26	2.00	7.29
W. ovata	1.09	0.37	0	11.11	1.99	0.32	3.62	18.23
Watznaueria sp.	1.08	0	0	20.00	3.52	0.57	4.42	23.45
HK-12/a								
C. mexicana mexicana	31.07	9.23	0	90.27	35.15	6.89	0.59	1.61
W. barnesiae	23.53	23.13	0	59.11	18.29	3.59	0.21	1.83
W. manivitae	14.90	2.97	0	52.38	18.87	3.70	0.95	2.24
C. margerelii	6.74	5.32	0	20.94	6.67	1.31	0.84	2.48
C. mexicana minor	2.89	0	0	50.00	9.93	1.95	4.35	21.05
W. biporta	2.46	0.38	0	25.00	5.40	1.06	3.14	13.01
Watznaueria sp.	1.88	0	0	22.22	5.02	0.98	3.12	12.13
W. fossacincta	1.84	0	0	12.50	3.46	0.68	2.06	6.17
C. argoensis	1.61	0	0	19.05	4.18	0.82	3.25	13.19
W. ovata	1.38	0	0	12.50	2.76	0.54	2.93	11.67
P. senaria/N. erbae	1.14	0	0	9.09	2.29	0.45	2.36	7.72
W. britannica	1.11	0	0	6.67	1.76	0.34	1.74	5.31

Elemental geochemistry

Mutual relations between selected main and trace elements were evaluated through their PCC's and coefficients of determination (R^2) (Table 3). Very good or good correlation with Al (>0.8) is suggestive of detrital origins of Ti, Ga, Rb, K, Zr, Fe and Th; besides, clastic connotations reveal also Ni, V, Mg and Co. Elemental concentrations of selected basic elements (Al, K, U, P and Ca) are presented on Fig. 5.

Table 2. Pearson's Correlation Coefficients between selected taxa in the Lókút LO-I (A), Hárskút HK-12/a (B) and Hárskút HK-12 (C) sections. Significant values ($P < 0.1$) are shown in bold. Correlations above 0.8 are indicated by grey cells; >0.9 by dark grey.

(A) LO-I	*C. argoensis*	*C. brezae*	*C. deflandrei*	*C. margerelii*	*Nannoconus* spp. top view < 10 m	*W. barnesiae*	*W. bayackii*	*W. biporta*	*W. britannica*	*W.* cf. *cynthae*	*W. fossacincta*	*Watznaueria* sp.
C. argoensis												
C. brezae	0.14											
C. deflandrei	−0.47	**−0.66**										
C. margerelii	−0.05	0.02	0.52									
Nannoconus spp. top view <10 µm	−0.19	0.44	−0.21	0.52								
W. barnesiae	−0.47	−0.51	**0.85**	**0.67**	0.22							
W. bayackii	−0.12	−0.13	−0.35	**−0.86**	−0.44	**−0.64**						
W. biporta	0.49	**0.69**	−0.41	0.06	−0.05	−0.48	−0.23					
W. britannica	−0.29	**−0.68**	0.16	−0.58	−0.37	0.03	**0.64**	**−0.66**				
W. cf. *cynthae*	−0.41	0.30	−0.08	−0.54	−0.43	−0.27	0.39	0.21	0.11			
W. fossacincta	0.2	0.08	**−0.72**	**−0.82**	−0.14	**−0.76**	**0.83**	−0.18	0.46	0.10		
Watznaueria sp.	0.42	−0.26	−0.43	**−0.74**	−0.54	**−0.64**	**0.76**	−0.21	0.49	0	**0.84**	

(B) HK-12/a	*C. argoensis*	*C. margerelii*	*C. mexicana mexicana*	*C. mexicana minor*	*P. senaria/ N. erbae*	*W. barnesiae*	*W. biporta*	*W. britannica*	*W. fossacincta*	*W. manivitae*	*W. ovata*	*Watznaueria* sp.
C. argoensis												
C. margerelii	**0.66**											
C. mexicana mexicana	−0.41	**−0.8**										
C. mexicana minor	**0.61**	0.33	−0.32									
P. senaria/N. erbae	0.27	0.28	−0.51	0.33								
W. barnesiae	0.43	0.84	**−0.98**	0.26	0.46							
W. biporta	**0.51**	**0.50**	**−0.60**	0.35	**0.88**	**0.59**						
W. britannica	**0.51**	**0.50**	−0.45	**0.79**	0.19	0.44	0.26					
W. fossacincta	**0.7**	**0.62**	**−0.49**	**0.86**	0.31	0.45	**0.49**	**0.84**				
W. manivitae	**0.75**	**0.54**	**−0.48**	**0.74**	0.39	0.40	0.45	**0.63**	**0.83**			
W. ovata	0.12	**0.63**	**−0.54**	0.05	0.46	**0.59**	0.43	0.16	0.20	0.13		
Watznaueria sp.	0.40	0.17	−0.32	0.77	0.41	0.21	0.43	**0.64**	**0.74**	**0.65**	−0.17	

(C) HK-12	*C. margerelii*	*C. mexicana mexicana*	*N. alvus*	*N. bronnimannii*	*N. infans*	*N. magnadiscus*	*N. steinmannii steinmannii*	*Nannoconus* (flat, small)	*Nannoconus* (narrow top canal)	*W. barnesiae*	*W. bayackii*	*W. biporta*	*W. britannica*	*W.* cf. *cynthae*	*W. ovata*	*Watznaueria* sp.
C. margerelii																
C. mexicana mexicana	0.22															
N. alvus	0.07	−0.22														
N. bronnimanni	0.04	−0.36	**0.49**													
N. infans	−0.28	−0.18	**−0.41**	−0.09												
N. magnadiscus	**−0.43**	−0.27	0	0.11	0.30											
N. steinmannii steinmannii	−0.06	−0.35	0	0.23	0.37	0.49										
Nannoconus (flat, small)	−0.13	−0.04	**−0.52**	−0.09	**0.54**	0.23	0.39									
Nannoconus (narrow top canal)	0.07	0.09	−0.18	0.01	**0.57**	−0.14	0.04	0.24								
N. barnesiae	−0.03	**0.41**	−0.01	**−0.49**	−0.48	−0.34	**−0.77**	−0.3	**−0.44**							
W. bayackii	−0.07	0.21	0.14	0.33	−0.32	0.01	−0.36	−0.21	−0.32	0.34						
W. biporta	−0.07	−0.3	0.16	0.07	−0.38	0.13	−0.14	**−0.47**	−0.23	−0.05	−0.22					
W. britannica	−0.18	−0.16	0.12	0.11	**−0.44**	**−0.46**	**−0.42**	**−0.54**	−0.34	0.33	0.22	0.29				
W. cf. *cynthae*	−0.24	0.14	−0.24	0.14	−0.06	−0.15	−0.23	0.02	−0.14	0.02	0.16	0.16	0.42			
W. ovata	0.15	−0.18	0.26	0.27	−0.45	−0.01	−0.5	**−0.45**	−0.18	0.23	0.30	**0.64**	0.19	−0.15		
Watznaueria sp.	0.01	−0.01	0.03	−0.15	−0.18	−0.23	−0.32	−0.25	−0.15	0.34	0.34	−0.05	0.01	−0.16	0.30	

Table 3. Pearson's correlation coefficients (PPC) and coefficients of determination (R^2) of elements examined in this study (combined for the Hárskút and Lókút successions). Grey shaded cells – moderate correlation (0.50–0.59); light blue shaded cells – good correlation (0.6–0.79); dark blue shaded cells, bold text – very good correlation (>0.8).

COEFFICIENTS OF DETERMINATION (R^2)

	Al	Ti	Ga	Rb	K	Zr	Fe	Ni	V	Mg	Th	Co	Cu	U	Ba	Zn	Mn	Ca	P	Na	
Al		**0.97**	**0.93**	0.75	0.71	0.67	0.66	0.59	0.56	0.55	0.40	0.37	0.12	0.09	0.09	0.06	0.00	0.00	0.01	0.26	Al
Ti	**0.98**		**0.93**	**0.95**	**0.95**	0.67	0.57	0.65	**0.84**	0.59	0.47	0.51	0.21	0.13	0.19	0.10	0.16	0.01	0.01	0.35	Ti
Ga	**0.97**	**0.97**		**0.93**	**0.91**	0.63	0.50	0.59	**0.81**	0.55	0.49	0.42	0.20	0.11	0.18	0.09	0.14	0.01	0.00	0.30	Ga
Rb	**0.86**	**0.97**	**0.96**		**0.94**	0.65	0.61	0.60	**0.88**	0.32	0.17	0.54	0.27	0.13	0.36	0.14	0.01	0.00	0.03	0.15	Rb
K	**0.85**	**0.97**	**0.96**	**0.97**		0.62	0.56	0.56	**0.81**	0.32	0.13	0.51	0.25	0.12	0.32	0.15	0.02	0.00	0.06	0.14	K
Zr	**0.82**	**0.82**	0.80	**0.80**	0.79		0.47	0.49	0.70	0.51	0.29	0.29	0.14	0.13	0.14	0.14	0.03	0.00	0.05	0.30	Zr
Fe	**0.81**	0.75	0.71	0.78	0.75	0.68		0.47	0.55	0.40	0.20	0.33	0.11	0.17	0.11	0.09	0.01	0.00	0.01	0.17	Fe
Ni	0.77	**0.81**	0.77	0.77	0.75	0.70	0.69		0.55	0.43	0.12	0.68	0.23	0.16	0.18	0.11	0.02	0.02	0.00	0.36	Ni
V	0.75	**0.92**	**0.90**	**0.94**	**0.90**	**0.84**	0.74	0.74		0.23	0.12	0.57	0.25	0.12	0.44	0.17	0.01	0.00	0.03	0.13	V
Mg	0.74	0.77	0.74	0.56	0.57	0.72	0.63	0.66	0.48		0.19	0.20	0.10	0.13	0.01	0.05	0.00	0.01	0.02	0.28	Mg
Th	0.63	0.68	0.70	0.42	0.36	0.54	0.45	0.35	0.35	0.43		0.05	0.01	0.00	0.00	0.01	0.12	0.00	0.00	0.24	Th
Co	0.61	0.72	0.65	0.73	0.71	0.53	0.57	**0.82**	0.76	0.45	0.22		0.24	0.13	0.38	0.24	0.01	0.00	0.00	0.29	Co
Cu	0.35	0.46	0.45	0.52	0.50	0.37	0.34	0.48	0.50	0.31	0.08	0.49		0.14	0.21	0.32	0.01	0.06	0.01	0.13	Cu
U	0.31	0.36	0.33	0.36	0.35	0.36	0.41	0.40	0.35	0.36	0.04	0.36	0.38		0.03	0.02	0.00	0.00	0.00	0.05	U
Ba	0.31	0.44	0.43	0.60	0.57	0.37	0.33	0.42	0.66	-0.08	0.00	0.61	0.46	0.16		0.27	0.02	0.00	0.00	0.02	Ba
Zn	0.24	0.32	0.29	0.38	0.38	0.37	0.30	0.33	0.41	0.23	-0.08	0.49	0.56	0.14	0.52		0.02	0.18	0.01	0.08	Zn
Mn	0.05	0.40	0.37	-0.08	-0.13	0.18	-0.10	0.16	-0.10	0.03	0.35	0.12	-0.10	0.07	-0.14	-0.13		0.08	0.12	0.05	Mn
Ca	-0.04	0.08	0.08	-0.02	0.00	0.00	0.01	0.12	0.06	-0.08	0.06	0.02	-0.25	0.02	-0.03	-0.42	0.27		0.00	0.00	Ca
P	-0.08	0.10	0.05	-0.18	-0.24	0.22	-0.10	0.01	-0.16	-0.13	0.06	0.00	-0.10	0.00	0.00	0.08	0.34	0.03		0.03	P
Na	0.51	0.59	0.54	0.39	0.38	0.55	0.41	0.60	0.36	0.52	0.49	0.54	0.35	0.22	0.16	0.28	0.22	-0.01	0.18		Na
	Al	Ti	Ga	Rb	K	Zr	Fe	Ni	V	Mg	Th	Co	Cu	U	Ba	Zn	Mn	Ca	P	Na	

PEARSON CORRELATION COEFFICIENTS (PCC)

COEFFICIENTS OF DETERMINATION (R^2)

Palaeoclimate proxies

Within the lower Tithonian of the Hárskút succession, Al/K is devoid of a clear trend (Fig. 6; Appendix S4). Above, at the Tithonian/Berriasian transition (magnetozones M19–M18), it becomes variable and generally elevated, to reach a minimum within the upper part of the lower Berriasian (M17r–M16r). An increasing trend is observed within the upper Berriasian–lower Valanginian (M16r–M13r); worth noting is also a local minimum in magnetozone M15. Characteristic of Ti/K (Fig. 6; Appendix S4) is a decreasing trend in the lower Tithonian–lower Berriasian (M22n–M16r), interrupted by a slight increase at the Tithonian/Berriasian boundary (M19n/M18r), as well as generally increasing values in the upper Berriasian–lower Valanginian (M16r–M13r). Also Th/K (Fig. 6; Appendix S4) decreases in the lower part of the succession (M22n–M17r); in this case, an interval of elevated values accounts for the upper Tithonian (M20n–M19n), characteristic is also a single peak in the upper part of M17r magnetozone. Above, within the upper Berriasian–lower Valanginian (M16n–M13r), Th/K increases; the trend is, however, less pronounced than in the case of Al and Ti based proxies. The CIA displays relatively stable values within the lower Tithonian and decreases above, in the upper Tithonian–lower Berriasian (M20n–M16r) (Fig. 6; Appendix S4). An increasing trend (interrupted by a slight negative peak within the magnetozone M15) is characteristic of the upper Berriasian, while the lower Valanginian depicts relatively high and stable CIA. Gallium/rubidium generally decreases through the Tithonian (M22n–M19n) and increases above, in the lower–lower upper Berriasian (top of M19n–M16n) (Fig. 6; Appendix S4). After the local minimum in magnetozone M15 it increases again towards the Valanginian (M15r–M13r). Finally, except for the single peak in magnetozone M22n, lower Tithonian Zr/Al are low and stable. It elevates in the upper Tithonian (M20n–M19r) and decreases through the lower Berriasian (M19n–M16r). Above, Zr/Al increases towards the Valanginian, having a local drop at the top of M14 (Fig. 6; Appendix S4).

The Lókút succession provides a corresponding record of palaeoclimate proxies, yet of significantly higher resolution in case of the upper Tithonian–lower Berriasian interval (Fig. 6; Appendix S4).

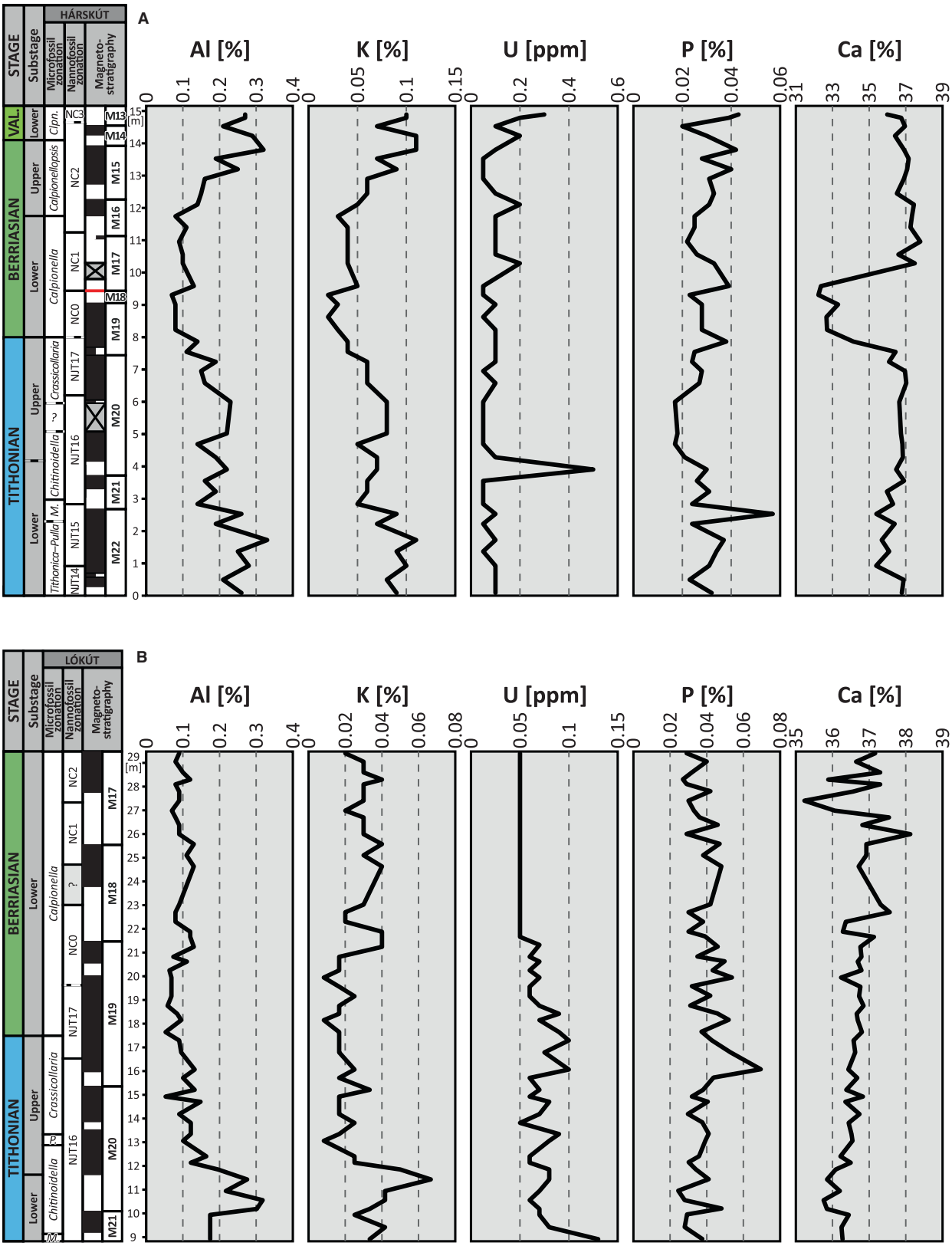

Fig. 5. Concentrations of selected detrital (Al and K), redox-related (U) and palaeoproductivity-related (P) elements, and Ca content in the Hárskút (A) and Lókút (B) successions. Abbreviations: VAL. – Valanginian; Clpn. – Calpionellites; M. – Mollucana; P. – Praetintinnopsella.

The lowermost part of the succession (M21n–M20n) is characterized by variable values of Al/K, devoid of a clear trend; above, within the upper Tithonian–lower Berriasian (M20n–M17n) it generally decreases, being interrupted by locally elevated values at the Tithonian/Berriasian boundary interval (M19n–M18r). Thorium/potassium manifests a decreasing trend, with locally elevated values in magnetozones M20n and M19n. Also CIA generally decreases through the succession (with a maximum value in M20r), depicting slightly elevated values within the lowermost Berriasian (M18). In the case of Ti/K, Ga/Rb and Zr/Al their record is available only for the lower Berriasian interval (M18r–M17n). There, Ti/K decreases, Zr/Al does not reveal any clear trend, whilst Ga/Rb reaches its maximum within the magnetozone M17r (Fig. 6, Appendix S4).

Redox-sensitive proxies

The Hárskút succession is characterized by very low (usually below 0.1 ppm) and stable concentrations of U, with a single peak in magnetozone M20r and an increasing trend at the top of the succession (Fig. 5). However, authigenic U (Fig. 7, Appendix S5) generally increases through the Tithonian–lower upper Berriasian (magnetozones M22n–M16n); the trend is however interrupted by a single peak in the uppermost lower Tithonian (M20r) and local drops (to ≤0) in magnetozones M20n, M18n and M17r. Besides, authigenic U notably decreases within the upper part of the upper Berriasian (M15r–M15n) and increases again at the top of the succession (M14r–M13r). Except for the local maximum in magnetozone M20r, enrichment factor (EF) U remains at a low and stable level within the lower–lower upper Tithonian beds (M22n–M20n; Fig. 7, Appendix S5). Above it is elevated at the Tithonian/Berriasian transition (M19r–M19n), decreases in the lowermost Berriasian (M18n–lower part of M17r) and rises towards the upper Berriasian. The uppermost Berriasian (M15n) is characterized by lowered EF U, whilst an increasing trend is observed

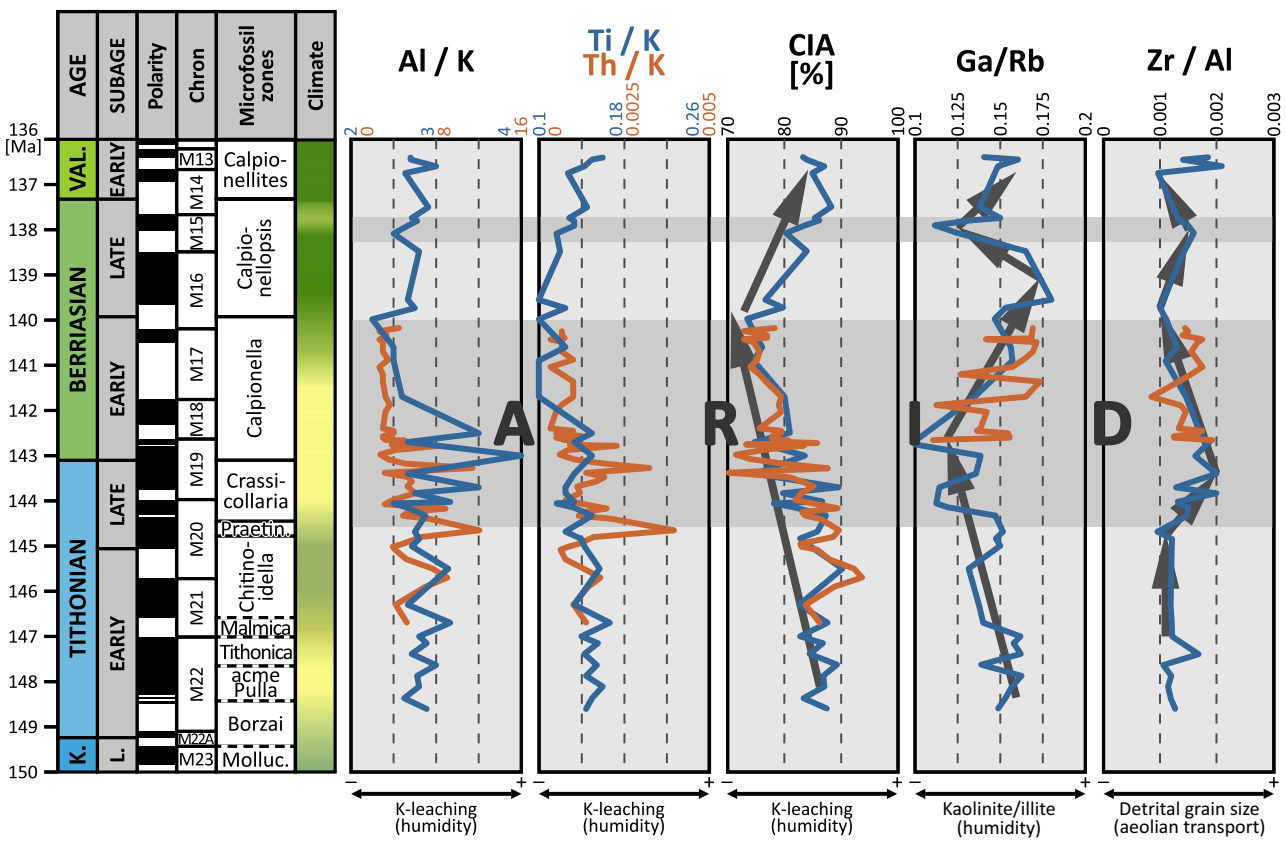

Fig. 6. Variations in selected palaeoclimate proxies during the Tithonian–early Valanginian in the area of Hárskút (blue) and Lókút (orange). Grey belts indicate intervals of climate aridization. Abbreviations: K. – Kimmeridgian; L. – Late; Molluc. – Mollucana; Praetin. – Praetintinnopsella.

at the top of the succession (M14r–M13n). In the case of Fe/Al (Fig. 7, Appendix S5) two intervals of elevated values can be noted: within the upper Tithonian–lowermost Berriasian (M20n–M18r) and at the lower/upper Berriasian transition (upper part of magnetozone M17r–M16n); these are separated by a local minimum in the lower part of magnetozone M17r. EF Mo (Fig. 7, Appendix S5) is variable through the Tithonian–lowermost Berriasian; however, one may notice a local maximum at the top of magnetozone M19n (uppermost Tithonian) and a local minimum within the lower part of magnetozone M17r. Above, the lower/upper Berriasian transition (upper part of M17r–lower part of M16n) is marked by a maximum in EF Mo; above – up to the top of the succession studied – it decreases.

Uranium concentrations generally decrease through the lower Tithonian–lower Berriasian of the Lókút succession, and are even lower than those of the Hárskút sections (below 0.1 ppm; Fig. 5). Authigenic U, in turn, depicts generally increasing content, with a slight drop in the upper lower Tithonian (M21n–M20r) and the lower part of magnetozone M17r (Fig. 7, Appendix S5). Also, EF U decreases within the upper lower Tithonian (M21n–M20r) and rises above, to reach its maximum at the Tithonian/Berriasian boundary (M19n). A decreasing trend – with a minimum at the bottom of magnetozone M17r (<2) – can be observed within the lower Berriasian beds, whereas slightly elevated EF U (*ca* 2) accounts for the top of the succession (M17r–M17n; Fig. 7, Appendix S5). Also, the Fe/Al curve provides a corresponding record, however it is devoid of a decreasing trend in the basal part of the succession (M21n–M20r; Fig. 7, Appendix S5). Finally, the basal part of the succession (magnetozones M21n–M19n) is characterized by relatively low EF Mo; those values rise significantly (to >20) only in the lowermost Berriasian (M19n/M18r). Above, in magnetozones M18n–M17r, EF Mo returns to low values, and rises again in the upper part of magnetozone M17 (Fig. 7, Appendix S5).

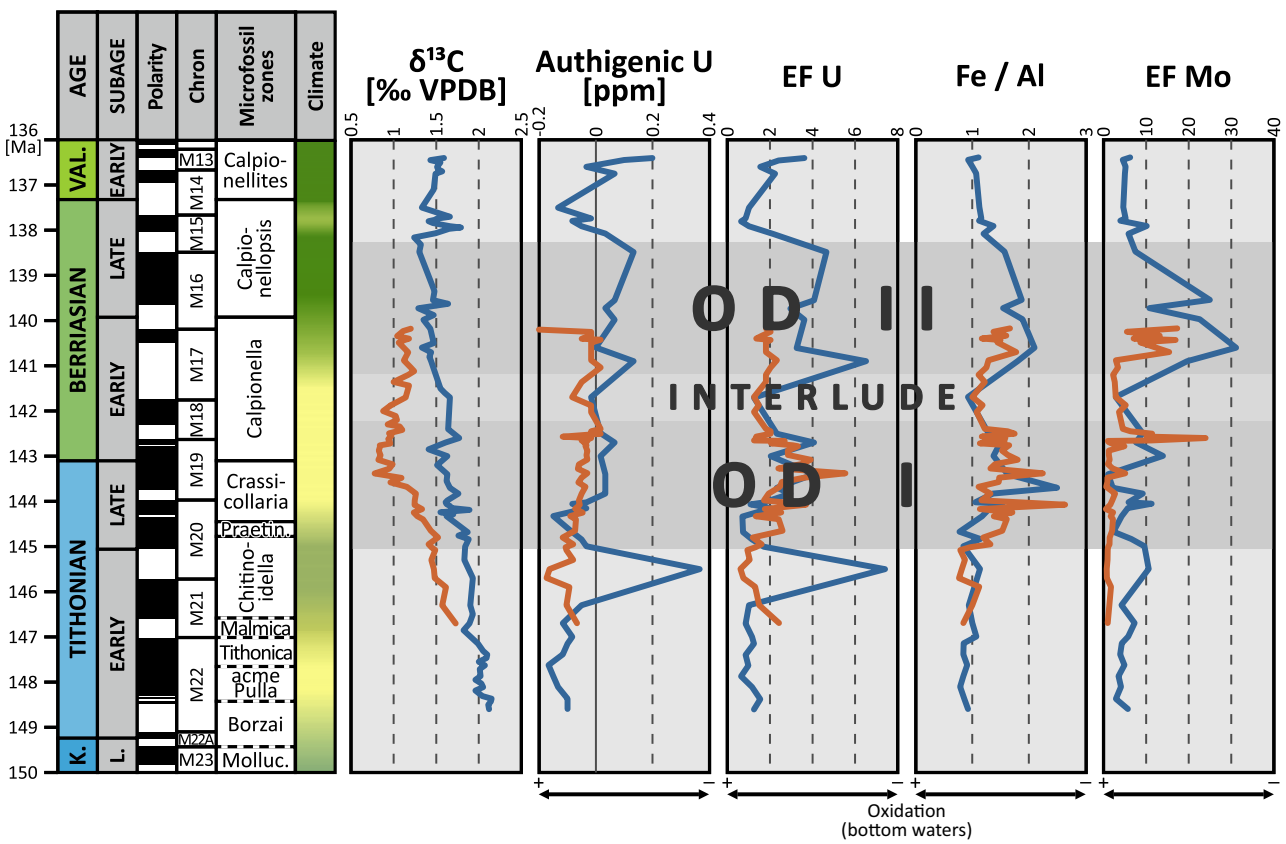

Fig. 7. Variations in selected redox (bottom-water oxidation) proxies during the Tithonian–early Valanginian in the area of Hárskút (blue) and Lókút (orange). Grey belts indicate intervals of oxygen deficiency (OD) at the seafloor. Abbreviations as on Fig. 5.

Micronutrient-type elements

The Hárskút succession is characterized by generally high enrichment in P (10 to 45; Fig. 8). In this context, EF P is relatively low and stable within the lower–lower upper Tithonian (M22n–M20n), and rises notably at the Tithonian/Berriasian transition (M19). It remains elevated up to the top of magnetozone M16r, whilst a clearly decreasing trend begins at the lower/upper Berriasian boundary interval (magnetozone M16) and continues up to the top of the succession studied (M13r). Corresponding trends describe also EF's of Ba, Zn and Cu; the most important differences are: (i) significantly higher (than in overlying beds) EF Zn and EF Cu at the Tithonian/Berriasian boundary interval (M19n–M18r); (ii) a local peak in EF Cu in magnetozone M22n (lower Tithonian) and in magnetozone M16n (upper Berriasian); and (iii) clearly increasing EF Zn and EF Cu at the top of the succession. It is noteworthy that a similar record, yet with a well-pronounced interval of lowered EF's in magnetozones M18n–lower M17r, is observed also in the Lókút succession (Fig. 8).

'Excess' P increases slightly at the bottom of the Hárskút succession, displaying a major peak in the upper part of magnetozone M22n, and gradually decreases above, towards magnetozone M20n (Appendix S6). P_{EXCESS} significantly elevates at the Tithonian/Berriasian transition (M19r–lower part of M17r), displaying a local minimum in magnetozone M18r. Above, a generally decreasing trend is observed; however, it is interrupted by elevated values in magnetozones M16n–M15n (upper Berriasian) and a major peak at the top of the succession studied (M13r). The above description relates also to variations in 'excess' Ba, Zn and Cu; the most important differences are: (i) their low concentrations within the upper Berriasian relative to the substrate; and (ii) local peaks in Ba_{EXCESS} and Cu_{EXCESS} in magnetozone M16, and – in the case of Cu_{EXCESS} – in the lower part of magnetozone M22n. Noteworthy, similar trends are observed also in P_{EXCESS}, Ba_{EXCESS}, Zn_{EXCESS} and Cu_{EXCESS}

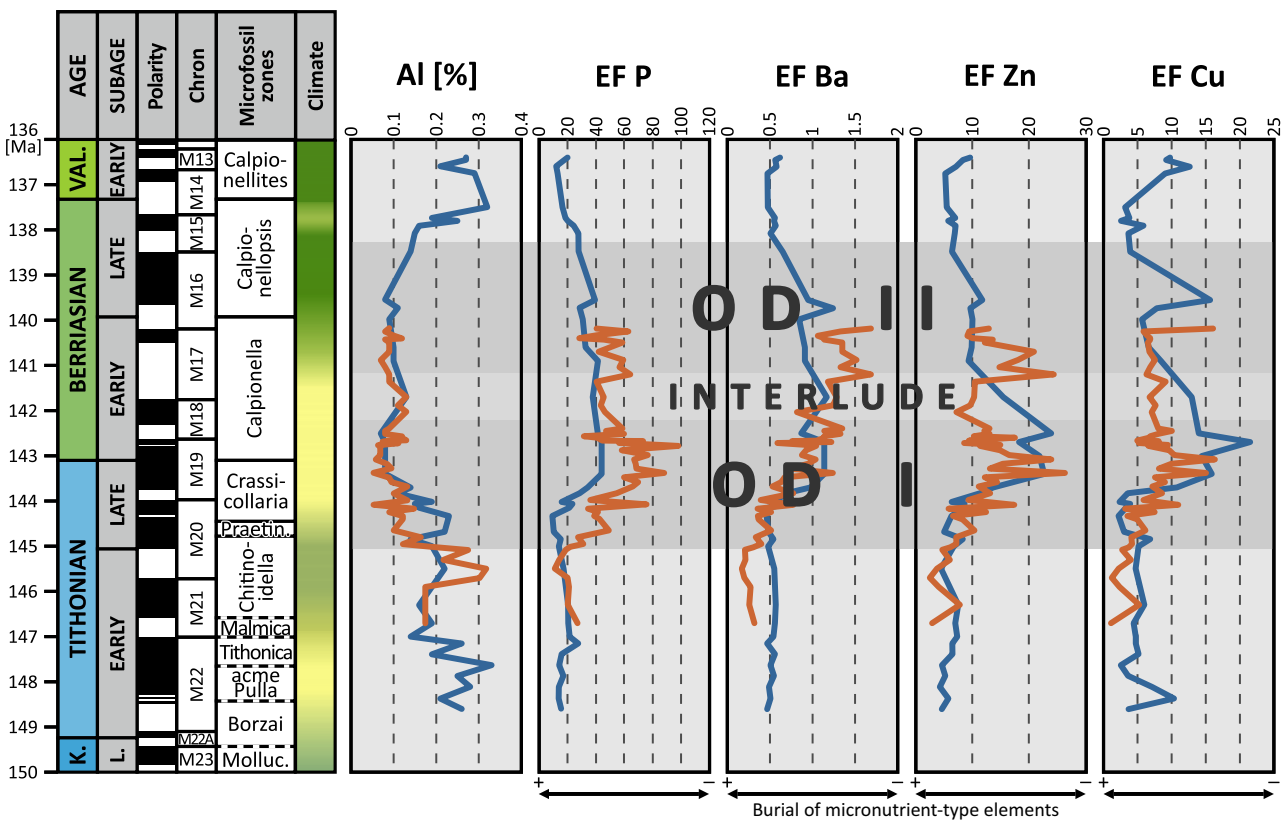

Fig. 8. Variations in Al content and burial of selected micronutrient-type elements (depicted as enrichment factor; EF) during the Tithonian–early Valanginian in the area of Hárskút (blue) and Lókút (orange). Note correlation between elevated EFs, decreasing lithogenic input (Al) and an interval of oxygen deficiency (grey belt, see also Fig. 6). Abbreviations as on Fig. 5.

curves from the Lókút succession; however, in this case increasing trends begin in a slightly lower stratigraphic position, at the base of magnetozone M20n (versus upper part of M20n in the Hárskút; Appendix S6).

Finally, accumulation rates of micronutrients to a large extent correspond to trends observed in their 'raw' (= not normalized to sedimentation rates) authigenic fractions, both in case of Hárskút and Lókút successions (compare Figs 8 and 9). The most important difference is notably elevated AR's (in relation to 'excess' content) within magnetozone M15 (compare Appendix S6 and Fig. 9).

INTERPRETATION

Calcareous nannofossil assemblages

As evidenced by very low TA values (Fig. 4), calcareous nannofossils are a rather scarce component of the Transdanubian Range sections (see also Stoykova in Grabowski *et al.*, 2017), in particular when compared with other Western Tethyan successions, either if those of similar (i.e. Southern Alps; Casellato, 2010) or different lithological appearance are considered (i.e. Western Balkan, consisting of marl and limestone alternations; Grabowski *et al.*, 2021b). Even though some samples demonstrate diagenetic effects, the general composition of the nannofossil assemblage is most likely original. Consequently, low observed TA values are considered as reflecting unfavourable environmental conditions for calcareous nannoplankton. Based on nannofossil relative abundances and diversity, both successions were divided into segments, each of presumably distinct palaeoecological meaning.

Lókút succession

The Tithonian–lowermost Berriasian (M21r–M19n) calcareous nannofossils of the Lókút succession were investigated by Stoykova in Grabowski *et al.* (2017). Although the method applied by the author prevents detailed statistical re-examination of this interval, RA variations of different nannofossil groups enabled division of

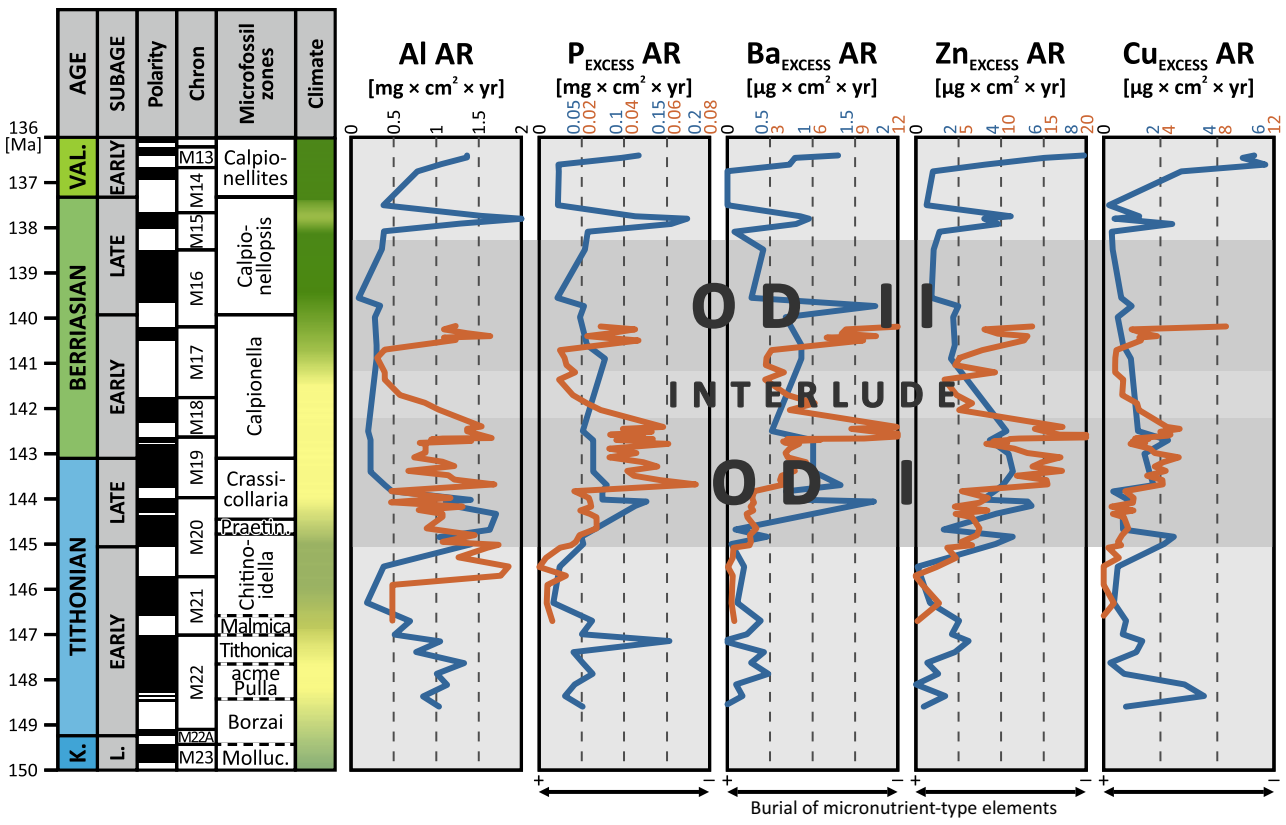

Fig. 9. Accumulation rates (AR) of Al and excess fraction of selected micronutrient-type elements during the Tithonian–early Valanginian in the area of Hárskút (blue) and Lókút (orange). Corresponding observations as in the case of Fig. 8 apply. Abbreviations as on Fig. 5.

two segments: L1 (M21r–M20r) and L2 (M20n–M19n; Fig. 4).

The lower one (L1; magnetozones M21r–M20r) is characterized by a dominance of *Conusphaera* spp. and corresponds to the NCE I event, *sensu* Casellato (2009) (Grabowski *et al.*, 2017; Lodowski *et al.*, 2022). The upper segment (L2; cf. M20n–basal M18r) covers an interval of a rapid rise of *Watznaueria* spp. (mostly *W. barnesiae*) and *Cyclagelosphaera* spp.; its upper part also covers the NCE II event of Casellato (2009), which is characterized by the recovery and dominance of *Conusphaera* spp. (M20n1n–M19n), as well as the disappearance of the genus at the base of magnetozone M18r (Fig. 4). According to Mattioli *et al.* (2014) the genus *Conusphaera* might have been a deep dweller proliferating during periods of stratification, whilst *W. barnesiae* is considered as eurytopic (see also Giraud *et al.*, 2016). Consequently, the nannofossil assemblage of the L2 segment is interpreted as reflecting a gradual stratification of the water column.

Collected data allow also to decipher a bipartite interval L3 (L3A and L3B on Fig. 4; M18r–M17n). The stratigraphically lower one (L3A) is marked by fluctuating and low values of TA and diversity (Fischer alpha between 3 and 6). Relatively abundant *C. margerelii* (up to *ca* 30%), which is considered as tolerant to salinity fluctuations (Tribovillard *et al.*, 1992), may result from increased evaporation (hence elevated salinity of the sea surface) under arid climate. The upper interval (L3B) has a similar composition, but manifests elevated TA, and slightly increasing – yet still low – diversity.

Hárskút succession

In the case of the Hárskút succession four intervals of possibly different palaeoecological meaning can be distinguished (H1–H4 on Fig. 4). The lower one (H1; lower Tithonian) is characterized by extremely low TA, fluctuating diversity, as well as domination of *W. barnesiae*, combined with various species of *Cyclagelosphaera*. Systematic vertical appearance of small and delicate forms such as *Polycostella*, *Hexalithus*, *Paleomicula* and *Rucinolithus* may suggest two phenomena: (i) that the original composition (assemblage) of nannofossils is preserved within the interval; or (ii) the higher proportion of delicate forms reflects elevated diversity, driven by enhanced availability of nutrients in the photic zone (see Püttmann & Mutterlose, 2021). In favour of the latter scenario is the dominance of *W. barnesiae*, which is considered the least oligotrophic taxon amongst the Jurassic *Watznaueria* pool (Giraud *et al.*, 2016), and which may reflect a relatively fertile photic zone of the early Tithonian ocean.

The overlying H2 segment (M20r–M19n) can be subdivided into two intervals: H2A and H2B. The H2A segment corresponds to the NCE I event (Bornemann *et al.*, 2003; Casellato, 2009), manifests distinct peaks in TA and a decrease in diversity, which may point to a specialized nannofossil assemblage. It is dominated by the genus *Conusphaera* (Fig. 4), suggestive of stratification and stable environment (Mattioli *et al.*, 2014). The H2B segment is characterized by a significant decline in TA and the record of the NCE II event in its upper part (= rise in nannoconids; Casellato, 2009).

The lower Berriasian H3 interval (M18r–M15r; Fig. 4) displays lowered TA's, fluctuating diversity and abundant *Watznaueria* spp.; distinctive also is a sharp decline of *Conusphaera* along with increasing share of *Nannoconus* spp. in its lower part. Nonetheless, due to unclear palaeoecological preferences of the genus *Nannoconus* (compare Erba, 2004 with Mattioli *et al.*, 2014 and Wulf *et al.*, 2020) the palaeoecological interpretation of this interval requires further studies.

Ultimately, characteristic of the H4 interval (Berriasian/Valanginian transition, M15n–M13r; Fig. 4) are elevated TA – predominantly related to the quick rise of a diverse nannoconid population – and fluctuating, yet still low diversity. Worth noting are also abundant forms of *N. steinmannii steinmannii*, which – according to Mattioli *et al.* (2014) – was tolerant to unstable conditions of a well-mixed water column. Besides, relatively frequent *C. margerelii* may indicate salinity stress.

Calcareous nannofossil assemblages: local correlation

Comparing calcareous nannofossil assemblages between the Hárskút and Lókút successions, one can notice some differences in their composition. The first issue, pointed out already by Lodowski *et al.* (2022), relates to slightly different stratigraphic positions of both the NCE I and NCE II events (Fig. 4). In the Lókút succession the NCE I event, which is characterized by the expansion of *Conusphaera* spp. (see Bornemann *et al.*, 2003), was documented from slightly older beds than in the case of the Hárskút (L1, M21n–M20r versus H2A, M20r–M20n; Fig. 4). Similarly, also the NCE II event (an increase in the number of nannoconids; Casellato, 2009) in the Lókút pre-dates the corresponding event in the Hárskút (upper part of L2, M19r–M19n versus H2B/H3, M19n–M18n). Also characteristic for the Lókút succession is a sharp decrease in *Conusphaera* spp. just above the

NCE I (lower part of L2, Fig. 4) and the following increase and dominance of the genus above. In the Hárskút succession *Conusphaera* spp. generally dominates up to the top of magnetozone M19n; however, an intermittent increase in *Watznaueria* spp. separates the two intervals dominated by *Conusphaera* within the magnetozone M20n1n (H2A/H2B transition on Fig. 4). Nonetheless, it is clear that in the case of both successions the relative share of *Conusphaera* spp. decreases drastically (and does not rebuild above) at the base of magnetozone M18r. Ultimately, the lower Berriasian (M18r–M17n) of both the Lókút (L3A–L3B) and the Hárskút (H3) successions is dominated by *Watznaueria* spp.; however, in the case of Hárskút also relatively high abundances of *Nannoconus* spp. are present. (Fig. 4).

Palaeoenvironment-related geochemical data

Palaeoclimate proxies

Relative variations in K content might relate either to kaolinite/illite proportions (where decreasing relative K indicates increasing content of kaolinite, hence humid palaeoclimate; e.g. Schneider *et al.*, 1997; Calvert & Pedersen, 2007; Tian *et al.*, 2011) and/or the illite/smectite ratio (where low K is suggestive of smectite, thus arid conditions; e.g. Diester-Haass *et al.*, 1993; Niebuhr, 2005). This research adopts the former as a basic mechanism behind the relative variations in K content, however a disclaimer is made for the Tithonian/Berriasian transition interval.

Accordingly, the K-leaching palaeoclimate proxies (Al/K, Ti/K, Th/K and CIA) depict two basic trends occurring in both the Hárskút and Lókút successions: (i) decreasing values in the upper Tithonian–lower Berriasian, suggestive of aridization; and (ii) increasing values in the upper Berriasian, indicative of a humid phase. Importantly, this scenario is consistent with variations in Ga/Rb (kaolinite/illite proxy) and Zr/Al (aeolian transportation proxy), which point to aridization climax during the earliest Berriasian (upper part of M19n). Besides, a relatively humid climate of the early/late Tithonian transition may be inferred from slightly elevated Al/K, Ti/K, CIA and Ga/Rb, whilst an occurrence of a short-lasting arid phase during the latest Berriasian (M15) is suggested by lowered Al/K, CIA and Ga/Rb, as well as an increase in Zr/Al (Fig. 6).

More complex is the issue of generally elevated and variable K-based indices within the Tithonian/Berriasian boundary interval (cf. magnetozones M19r–M18n; Fig. 6). By adopting the mechanism of hydrolysis-related variations in relative K content, this phenomenon should be interpreted as suggestive of temporal humidification. However, such a scenario appears unlikely when considering other palaeoclimate proxies and published data. Accordingly, arid climate during the Tithonian/Berriasian transition is evidenced by: (i) evaporites and clay mineralogy of various northern European successions (i.e. Hallam *et al.*, 1991; Hesselbo *et al.*, 2009; Grabowski *et al.*, 2021a; see also Schneider *et al.*, 2018); (ii) evaporitic structures and clay mineralogy of the Jura Mountains (Rameil, 2005); (iii) clay minerals of the Vocontian Basin (south-east France, Morales *et al.*, 2013); and (iv) palynofacies and clay minerals of the central Tunisia sections (Schnyder *et al.*, 2005). On this basis it is considered that elevated K proxies at the Tithonian/Berriasian transition might result from: (i) increased share of aeolian fraction delivered from different source areas (= possessing different proportions of examined elements); and/or (ii) cessation of hydrolysis on lands, connected with a temporal 'switch' of K-based proxies to illite/smectite mode.

Palaeoredox proxies

Low computed authigenic U in both Hárskút and Lókút sections is suggestive of uninterrupted oxic sea bottom conditions (compare Fig. 7 with Jones & Manning, 1994). However, according to Algeo & Liu (2020), palaeoredox classification of U-based proxies by Jones & Manning (op. cit.) should not be directly applied when examining different sedimentary successions. On this basis, a coherent record of palaeoredox proxies – either when considering different proxies and/or comparing between the studied successions – as well as relatively high EF U (even >6), Fe/Al (usually 1 to 2) and EF Mo (up to 30) (Fig. 7) are thought to document real changes in seafloor oxygenation.

Accordingly, collected data document two intervals deposited under the limited availability of oxygen (hypoxia): (i) the upper Tithonian–lowermost Berriasian (OD I, magnetozones M20n–M18r); and (ii) the lower/upper Berriasian transition (OD II, upper part of magnetozone M17r–M16n). They are separated by a relatively short 'interlude' interval (M18n–lower M17r). It must be also emphasized that OD I and OD II 'events' were hypoxic (= they record decreased availability of oxygen under a generally oxic regime), and should not be confused with anoxic conditions, because oxic conditions are evidenced by continuous occurrence of benthic organisms (i.e. benthic foraminifera; see fig. 5 in Lodowski *et al.*, 2022; see also Vörös *et al.*, 2020).

Intriguing are also the distinct uppermost lower Tithonian (M20r) peaks in U proxies, which occur only in Hárskút (Fig. 7). Besides, Fe/Al and EF Mo curves are devoid of such a peak in both studied successions. Consequently, elevated accumulations of U were most likely unrelated to seafloor oxygenation and more likely resulted from prolonged exposure of the seafloor (for instance, due to stratigraphic condensation) to uranyl ions (see Tribovillard *et al.*, 2006). However, the considered horizon is devoid of any peak in lithogenic admixture (which should occur in regimes of lowered sedimentation rates; see Al and K on Fig. 5), therefore unequivocal interpretation of this phenomenon cannot be made.

Micronutrient-type elements

Trends recorded in EF's (Fig. 8) and 'excess' concentrations of P, Ba, Zn and Cu (Appendix S6) – and, to some extent, their AR's (Fig. 9) – depict three characteristic intervals, characterized by: (i) elevated values at the Tithonian–Berriasian transition (M19r–M18r); (ii) lowered values in mid lower Berriasian (M18n–lower part of M17r); and (iii) another high at the lower/upper Berriasian transition (upper part of M17r to 16n). These phenomena not only correlate between the Hárskút and Lókút successions, which allows to infer about their regional (= at least basinal in scale) importance, but are also isochronous with OD I and OD II events (compare Fig. 7 with Figs 8 and 9). This, in turn, enables the assumption that intensity of micronutrient burial might have been directly related to mechanisms controlling the availability of oxygen at the bottom of the Bakony Basin.

Relatively low AR's in the upper Berriasian of the Hárskút succession (Fig. 9), in particular within magnetozone M16n, are most likely related to a condensation horizon documented by Lodowski *et al.* (2022). Due to the fact that sedimentation rates are calculated for the entire magnetozone – in this case both the interval below and above the condensation zone – the actual deposition rates of uncondensed intervals were higher than computed; this in turn, directly translates into relatively low AR's.

DISCUSSION

Tithonian–early Valanginian palaeoenvironment of the Transdanubian Range

Integration and correlation of geochemical data with the palaeoecological record provided by calcareous nannofossils (Fig. 4) enabled a consistent interpretation of the Tithonian–early Valanginian palaeoenvironment evolution in the area of the Transdanubian Range.

Early Tithonian

This study points to a rather humid climate of the early Tithonian (relatively high values of K-leaching proxies and Ga/Rb; Fig. 6). This is in agreement with both the Tethyan (Rameil, 2005; Bover-Arnal & Strasser, 2013) and Subboreal (i.e. Hesselbo *et al.*, 2009) data, which evidence relatively humid early Tithonian and an arid Tithonian/Berriasian transition. Taking into account that continental configuration during the Mesozoic was propitious for strong monsoons ('megamonsoons', see De Wever *et al.*, 2014, and references therein), and that the Transdanubian Range was located at favourable latitudes for such a process (*ca* 10° to 15° N; Lodowski *et al.*, 2022), it is considered that in the Bakony Basin humid phases might have been connected with monsoon-induced upwellings and/or downwellings (either the nearshore – 'Ekman', or seafloor obstruction type; see e.g. Trujillo & Thurman, 2011). Such a configuration ensured a well-mixed water column; hence not only a well-oxygenated seafloor (for example, low EF U on Fig. 7), but also an effective mechanism of nutrient shuttle (uptake) (Figs 8 and 9), as evidenced also by the rather nutrient-prone (possibly mesotrophic) nannofossil assemblage (H1) in the Hárskút succession (Fig. 10; see also Fig. 11).

Somehow problematic is the issue of non-isochronous peaks in 'productive' elements within magnetozone M22n (Figs 8 and 9). These occurred under decreasing clastic influx, and therefore were most likely related to other processes, i.e. periodic disturbances in water mixing. The latter, in turn, might have been connected with aridization (see a single drop in Ga/Rb and a peak in Zr/Al within M22n magnetozone; Fig. 6) and – related – less efficient monsoonal upwellings during the so-called 'Hudlestoni' event (e.g. Wignall & Ruffel, 1990; Hesselbo *et al.*, 2009). This phenomenon was already correlated with the High-Tatric succession (Lodowski & Grabowski, 2023), which may serve as indirect evidence for a possibly wider (exceeding the Subboreal Europe) range of this climatic event. For these reasons, the above hypothesis requires further investigations.

Late Tithonian–early Berriasian

Several authors have documented climate cooling during late Tithonian–(possibly)early Berriasian (Gröcke *et al.*, 2003; Weissert & Erba, 2004;

Tremolada *et al.*, 2006; Tennant *et al.*, 2016; Baumgartner *et al.*, 2023; see also discussion in Price *et al.*, 2016). Moreover, the first occurrence of dropstones in the Sverdrup Basin (Arctic Canada; Schneider *et al.*, 2020) can be roughly approximated to *Dorsoplanites ilovaiskii* Northern Siberian ammonite Zone, and the *Fallauxi*/*Ponti* Tethyan ammonites zonal boundary (cf. upper part of M20r magnetozone; see Turner, 2018; Hesselbo *et al.*, 2020). This, in turn, suggests that climate cooling had begun already during the latest early Tithonian. In this context, cool climate is known to reduce the thermal gradient between continents and the ocean, which also lowers the intensity of the atmospheric circulation (Trujillo & Thurman, 2011). Such conditions are not only favourable for aridization, but also – due to less intense monsoons – could result in weakened efficiency of upwelling/downwelling induction. The above is also in agreement with Casellato (2009), who considered that the increase in size and calcification of the calcareous nannoplankton during the late Tithonian might have been stimulated by low oceanic Mg/Ca ratio, low pCO_2, as well as the climate cooling and aridization (see also Abbink *et al.*, 2001).

In the Transdanubian Range, the onset of an arid climate mode can be traced already within the lowermost upper Tithonian beds (i.e. decreasing CIA on Fig. 6; see also Appendix S4). This process might have resulted in weakened atmospheric circulation and less efficient upwellings. As a result of restrictions in water mixing, not only did the seafloor become depleted in oxygen (OD I on Fig. 7), but also a higher amount of micronutrients was subjected to burial (OD I on Figs 8, 9, and 11). This interpretation is supported also by the fact, that the late Tithonian–early Berriasian was a time of very limited lithogenic influx (Al on Figs 8 and 9), therefore elevated nutrient accumulations must have been related to oceanographic processes, not the continental runoff. Marine stratification during this time is additionally evidenced by a frequent *Conusphaera* spp. (L2 and H2 on Fig. 10).

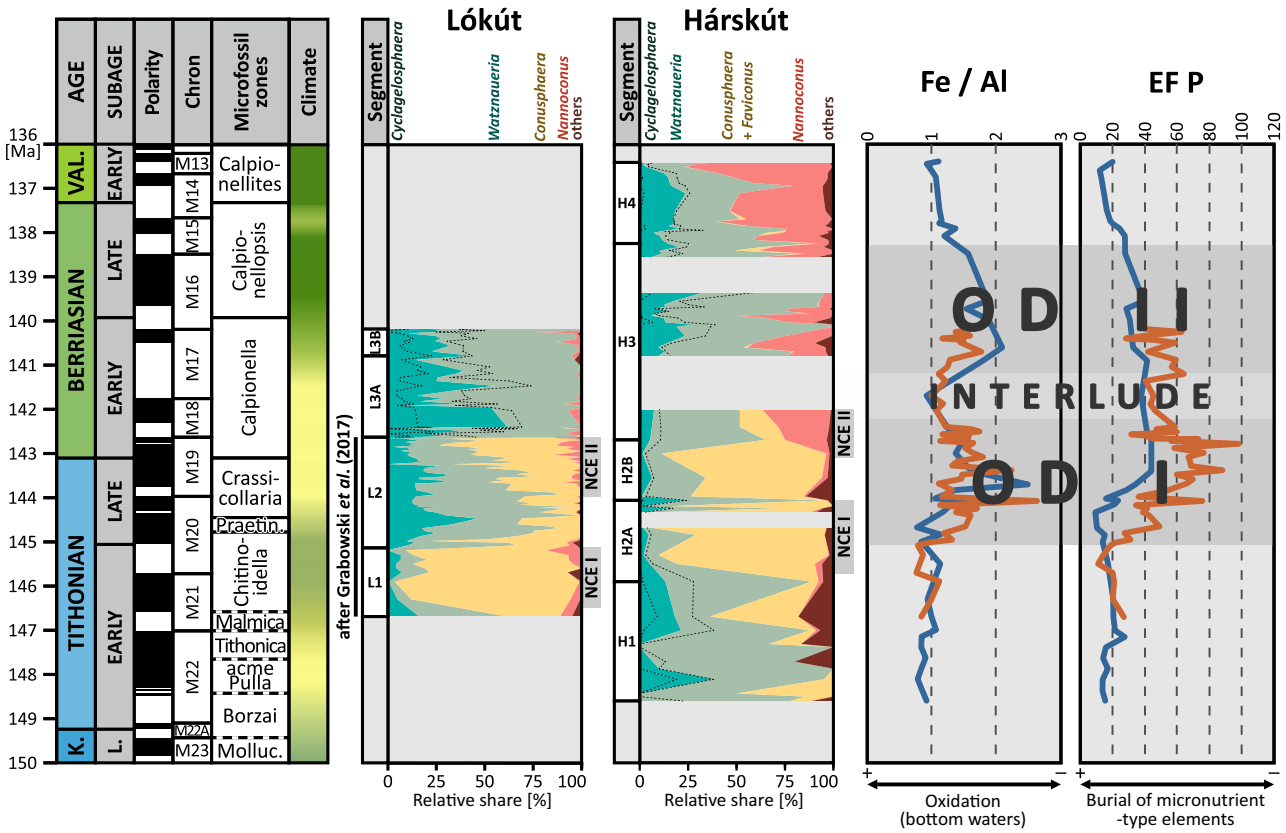

Fig. 10. Time-domain correlation of changes in calcareous nannofossils assemblages (relative abundances of five selected groups), Fe/Al (palaeoredox proxy) and enrichment factor (EF) P (burial of micronutrient-type elements proxy) in the Lókút and Hárskút successions.

Such conditions prevailed until the mid-early Berriasian (M18n–lower part of magnetozone M17r), which was characterized by progressing aridization (Fig. 6), yet relatively oxic seafloor ('interlude' on Fig. 7) and low burial of trace metals (Figs 8 and 9). In this case, progressing climate cooling is considered to allow the pressure gradient between continents and the ocean to reach the threshold, beyond which vertical water circulation might have been temporarily driven either by Walker-type circulation or dry offshore winds (Trujillo & Thurman, 2011). In this context, a drastic decline of genus *Conusphaera* by the end of the OD I event (L3 and H3; Fig. 10) might have resulted from a temporal change in trophic state and the state of the water column, presumably due to increased water mixing at the base of M18r.

Late Berriasian

Interpretation of the upper Berriasian data is not straightforward. As inferred from the geochemical data (Fig. 6), during the early/late Berriasian transition the Transdanubian Range was subjected to humidification. Such conditions are favourable for intense monsoonal circulation, hence effective mixing of the water column; however, rather weak oxidation of the sea bottom and relatively high accumulations of micronutrients within the upper part of magnetozone M17r–M15r suggest the opposite (i.e. stratification of the Bakony Basin, OD II on Figs 7 to 9).

This apparent contradiction can be explained when taking into account the late Berriasian tectonic reactivation in the Neotethyan Collision Belt (i.e. Gawlick *et al.*, 2009; Fodor *et al.*, 2013; Lodowski *et al.*, 2022; see also Nozdrovice event in Michalík, 2007). This process involved the formation of an island arc, which might have acted as a barrier separating the Alpine Atlantic from the Neotethys Ocean *sensu stricto* (see Fig. 1). As a result, the Bakony Basin might have been effectively cut off from monsoonal upwelling/downwelling processes, which took place on the Neotethyan margin of the NCB (Fig. 11). It is noteworthy that palaeoenvironmental perturbations during the early/late Berriasian transition are evidenced also by a brachiopod fauna. The three-step turnover and the final (late Valanginian) extinction of pygopid fauna was documented by Vörös *et al.* (2019, 2020), whilst Vörös & Szives (2023) linked the late Valanginian crisis to nutrient oversupply and dysoxic conditions during the 'Weissert' event. In light of the present study, also the mid-Berriasian crisis can be explained by enhanced nutrient accumulations and the seafloor hypoxia during the late Tithonian–early Berriasian OD I and OD II events (Figs 7 to 9).

The mid late Berriasian (magnetozone M15r) brought back relatively intense mixing of the water column (i.e. low EF U and EF Ba on Figs 7 and 8), followed by an expansion of nannoconids (H4 on Fig. 10). During this time NCB likely still acted as a physical barrier between the Neotethys *ss.* and Alpine Atlantic (as suggested by consecutively increasing contribution of terrigenous fraction; see Al and K on Fig. 5), therefore monsoonal circulation should be excluded also in this case from factors controlling the water mixing in the former. Alternatively, the combination of the humid climate of the late Berriasian and elevated position of the NCB, might have resulted in development of an internal (= specific for the Alpine Atlantic) current system, which may have ensured sufficient water mixing. Additionally, continental fluvial runoff during the humid phase might have increased the importance of riverine supply of nutrients (see Baumgartner, 2013). Interestingly, the well-mixed state of the water column and relatively high clastic input (possibly nutrient availability) during the late Berriasian was apparently harmless for the genus *Nannoconus*, which proliferated during this time (H4 on Fig. 4).

Also characteristic for the latest Berriasian of the Transdanubian Range was a short-lasting arid phase (M15r/M15n magnetozonal boundary, Fig. 6). Nonetheless, it likely had a limited impact on oceanographic conditions prevailing in the Bakony Basin, in particular water column mixing, as evidenced by the signal of oxic seafloor (Fig. 7). In turn, significantly increased accumulation rates of micronutrient-type trace metals (Fig. 9) correlate with higher nannofossil TA (Fig. 4), suggestive of an actual increase in sea-surface primary productivity. These phenomena might have been triggered by elevated supply of clastic material (= nutrients; Al on Fig. 9) during a time when vegetation cover was restricted by progressing climate aridization (see Kraus *et al.*, 2015).

It should also be noted that the condensed character of the upper Berriasian of the Hárskút succession (for example, limited thickness of magnetozone M16n) translates into limited resolution of the available data. Consequently, the OD II 'event' of this study can in fact encompass a higher number of environmental perturbations. For instance, in Barlya (Peri-Moesian Basin, Bulgaria) dysoxic conditions lasted only until the earliest late Berriasian (M16r), however some traces of hypoxia can be followed also within the mid part of magnetozone M16n (Grabowski *et al.*, 2021b).

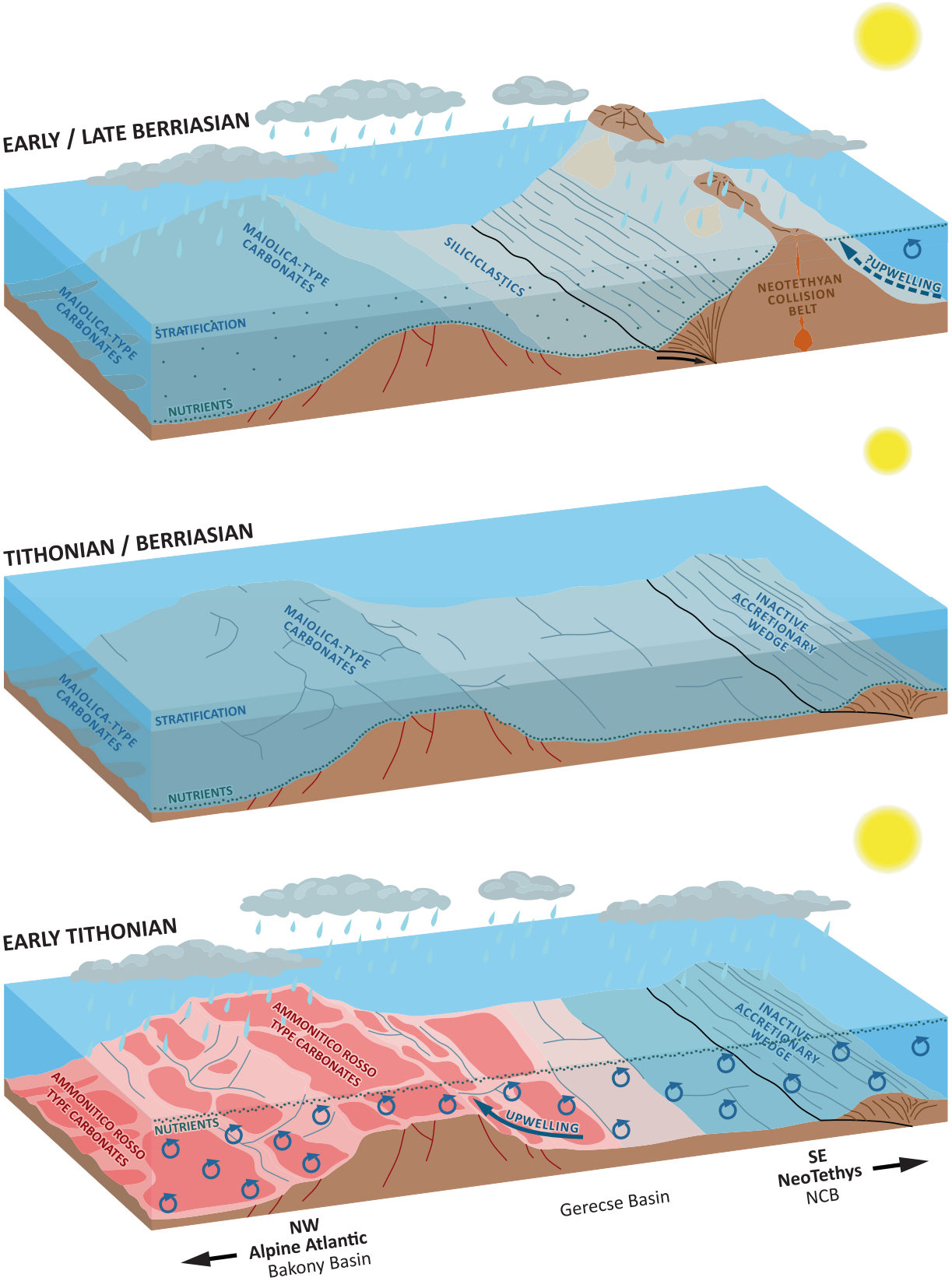

Fig. 11. Palaeoenvironmental reconstruction of the Transdanubian Range during the early Tithonian, Tithonian/Berriasian and the early/late Berriasian transition.

Accordingly, elevated yet significantly variable TA and RA of *N. steinmannii steinmannii* (H4 on Fig. 4; Appendix S2) may result from an unstable marine environment, as suggested by Mattioli *et al.* (2014; compare with Erba, 1994; Bornemann *et al.*, 2003; Wulf *et al.*, 2020).

Early Valanginian

The Berriasian/Valanginian transition beds (magnetozone M14r) indicate humid climate (Fig. 6), oxic sea bottom conditions (Fig. 7) and low nutrient accumulations (Figs 8 and 9). Such a record is suggestive of effective water mixing, most likely due to similar mechanisms/processes such as during the late Berriasian.

Later chrons (M14n–M13r) are characterized by elevated U proxies (Fig. 7) and trace metal content (Figs 8 and 9). However, palaeoclimate proxies point to uninterrupted humid climate (Fig. 6), which corresponds well with reports from the Vocontian Basin (Morales *et al.*, 2013; Charbonnier *et al.*, 2016). Accordingly, high accumulation rates of micronutrients are considered here as predominantly related to high influx of the clastic fraction under the humid climate regime (compare with Al on Fig. 9). Consequently, such a record is thought to evidence an actual increase in the sea-surface productivity. In turn, relatively high values of U-based palaeoredox indices might have resulted from extremely low sedimentation rates and prolonged exposure of the seafloor to uranyl ions (see Tribovillard *et al.*, 2006). This assumption is based on the fact that the level of stratigraphic condensation documented by Főzy *et al.* (2010; bed 10 therein) is the very same stratigraphic horizon as the one with elevated values of U indices (bed HK-46 herein).

Calcareous nannofossils versus the geochemical record

When comparing the geochemical record of the palaeoenvironment with nannoplankton communities, one may notice that there is no systematic correlation between changes in nannofossil assemblages and the amount of palaeoredox-related and/or micronutrient-type elements (Fig. 10). On one hand, *Watznaueria* spp. dominate the lower Tithonian of the Hárskút succession (H1), which was characterized by high clastic influx (Al on Fig. 8) and the well-mixed water column (Fig. 10). On the other, they are dominant also within the lower Berriasian of both Hárskút (H3) and Lókút (L3), therefore the interval recording the switch from the mixed (interlude on Fig. 10) to stratified Bakony Basin (OD II on Fig. 10), as well as the minimum lithogenic input (Al on Fig. 8). Consequently, most likely *Watznaueria* spp. were not related to the state of the water column (mixed *versus* stratified) and/or the nutrient supply in a direct and simple way (see also Giraud *et al.*, 2016).

One may notice that the expansion of *Conusphaera* spp. (NCE I; L1, H2A) is not only diachronous between the successions, but also do not manifest in the geochemical record (Fig. 10). Accordingly, even though *Conusphaera* is considered as having an affinity to the stratified water column (Mattioli *et al.*, 2014), the NCE I event might have been triggered by different palaeoceanographic factors (i.e. global-scale changes in oceanic chemistry), which led to the first period becoming generally favourable for biocalcification oceanographic conditions (see Bornemann *et al.*, 2003; Tremolada *et al.*, 2006; Casellato, 2009). This assumption is supported by the fact that Tremolada *et al.* (2006) documented the NCE I event from a single distinct peak in *Conusphaera* spp. at the lower/upper Tithonian boundary of the Central Atlantic Ocean (cf. magnetozone M20), above which their numbers consecutively decrease towards the Berriasian. In turn, in the case of the Alpine Atlantic realm, *Conusphaera* spp. partly regain in abundance within the upper Tithonian (compare Fig. 10 with Brodno and Tré Maroua sections; Michalík *et al.*, 2009, Grabowski *et al.*, 2022). On this basis, the NCE I event can be interpreted as a manifestation of the pioneer character of genus *Conusphaera*, presumably resulting from their ability for effective colonization (more effective in comparison to other genera).

On other hand, the resurgence of *Conusphaera* is not only isochronous in the Transdanubian Range sections, but it also coincided with stratification in the Bakony Basin (OD I on Fig. 10). Such a record suggests that the change in the nanoplankton community might have been driven by oceanographic perturbations (stratification-induced oligotrophy). The relation between the two processes is most likely evidenced also by the sharp decline in *Conusphaera* at the basal Berriasian, which coincided with a termination of the OD I event (Fig. 10). Accordingly, the relative dominance of *Conusphaera* spp. during the latest Tithonian–earliest Berriasian may document their specialized life strategy, that is affinities to a highly oligotrophic water column (see Mattioli *et al.*, 2014), but also noncompetitive character of the genus (= narrower environmental tolerance than i.e. *Watznaueria* spp.).

The above considerations will be supplemented with additional statistical evaluations and discussed in detail in a separate paper.

Implications for carbon cycling

The Tithonian–Berriasian of the Transdanubian Range is characterized by consecutively decreasing $\delta^{13}C$ (Fig. 7; see also Price *et al.*, 2016, and Lodowski *et al.*, 2022). However, the upper Tithonian (M20n1n–M19n2n) manifests a well-pronounced drop in ^{13}C, in particular in the case of the Lókút succession. As this phenomenon corresponds to the OD I event documented in this study (compare, for example, to EF U on Fig. 7), it is considered that relatively light carbon signatures were driven by stratification and low productivity of the upper ocean, which resulted in lowered biotic demand for ^{13}C. This is in agreement with Košťák *et al.* (2023), who discussed the possible relation between the negative carbon shift at the Colomi/Alpina subzonal boundary (mid M19n2n), oligotrophication and climate aridization. Accordingly, slightly increasing $\delta^{13}C$ within the lower Berriasian of the Lókút succession (upper M19n–lower M17r; 'interlude' on Fig. 7) are thought to result from enhanced water mixing during the 'interlude' event and associated increase in primary productivity (compare with Figs 8 and 9). It is noteworthy that a much less pronounced record of this phenomenon can be followed also within the Hárskút succession, in magnetozone M18n (Fig. 7), which suggests higher sensitivity of deeper deposition zones to this kind of perturbation. Besides, the topmost beds of the Lókút succession (upper M17r–M17n) – similar to the entire OD II interval in Hárskút – depict slightly decreasing $\delta^{13}C$, which might result from another decrease in demand for ^{13}C. Finally, a notable increase in carbon signatures within the uppermost Berriasian of the Hárskút succession (magnetozone M15; Fig. 7) correlates well with the interval of elevated surface productivity (see discussion above; compare Figs 7 and 9) and – presumably – lower availability of ^{12}C. Based on the above, it is interpreted that the latest Jurassic–earliest Cretaceous carbon cycle in the Bakony Basin was to large extent dependent on climate-controlled marine circulation and trophic state.

Vanishing of *Saccocoma*

The disappearance of *Saccocoma* microfacies within the upper Tithonian beds (cf. M19r/M20n magnetozonal boundary; e.g. Lodowski *et al.*, 2022) is a well-known western Tethyan phenomenon. This process was correlated with the NCE II event of Casellato (2009) by Grabowski *et al.* (2019), which suggested that palaeoenvironmental processes contributing to the NCE – such as climate changes, pCO_2 and/or Mg/Ca ratio in the seawater (Bornemann *et al.*, 2003; Tremolada *et al.*, 2006; Casellato, 2009) – might also have been important to those planktonic crinoids. However, when also considering the data collected during this study, it can be noticed that their vanishing (as well as the NCE II event) was simultaneous with climate aridization. Consequently, if the model proposed in this research – that is a direct connection between the climate conditions (humid/arid), state of the water column (mixed/stratified) and the nutrient shuttle system (their uptake/burial) – is followed, the disappearance of *Saccocoma* can be interpreted as resulting either from an insufficient (= below their tolerance) amount of micronutrients in the upper ocean and/or the state of the water column itself (= degree of stratification/water mixing). Nonetheless, as in the case of the Transdanubian Range, saccocomids become rock forming only during the Tithonian, that is after the termination of 'productive' (= radiolarian) ocean (i.e. Szederkényi *et al.*, 2013), they should be considered as generally oligotrophic.

CONCLUSIONS

Integration of geochemical data (Figs 6 to 9) with analysis of calcareous nannofossil assemblages (Figs 4 and 10), in particular their consistent and complementary record between the Hárskút and Lókút successions, enabled reconstruction of the Tithonian–early Valanginian palaeoenvironment of the Bakony Basin and its evolution.

1 The process of the late Tithonian–early Berriasian climate aridization – so far best known from the Subboreal realm – was documented in geochemical data (lowering values of K-leaching proxies and Ga/Rb, as well as increasing Zr/Al; Fig. 5) and – indirectly – in nannofossil assemblages, which are dominated by heavily calcified forms (Fig. 4; compare with Casellato, 2009). This phenomenon is thought to result from climate cooling, when decrease in thermal gradient between continents and the ocean might have weakened the atmospheric circulation decreasing also the humidity.

2 The interval deposited under the arid climate is characterized by elevated values of palaeoredox indices, as well as relatively high concentrations of micronutrient-type trace metals (OD I on Figs 7 to 9). Such a record is interpreted as resulting from decreased efficiency of wind (monsoon) induced water mixing, which drove the stratification of the Bakony Basin. This, in turn, restricted the vertical transportation of oxygen and disrupted the nutrient shuttle (uptake) mechanism (Fig. 11). Such a scenario is consistent with the upper Tithonian–lowermost Berriasian domination of genus *Conusphaera*, which was linked to the stratified water column by Mattioli *et al.* (2014).

3 The well-known late Berriasian climate humidification is clearly expressed in geochemical indices (increasing trends in K-based proxies and Ga/Rb, lowered Zr/Al; Fig. 6). However, this phenomenon apparently did not translate into oceanographic change, being significantly reduced by the (roughly) simultaneous tectonic uplift of the Neotethyan Collision Belt. Due to the formation of the physical barrier separating the Alpine Atlantic from the Neotethys Ocean *ss.*, the Bakony Basin is thought to have been subjected to prolonged stratification of the water column, seafloor hypoxia and intensified burial (accumulation) of micronutrients (OD II on Figs 6 to 9 and 11). Nonetheless, the OD II interval was presumably more multi-staged and heterogenous than indicated by the record of the Hárskút composite section (see Grabowski *et al.*, 2021b).

4 The inferred scenario is in agreement with palaeoclimate data coming from other European successions, either from Subboreal or Tethyan provenance; this allows to consider the over-regional importance of palaeoenvironmental perturbations discussed herein. Besides, OD I and OD II events were correlated with local lows in carbon isotope signatures (Fig. 7). The latter suggests the importance of local/regional marine circulation for the carbon cycle, in particular the productivity-driven demand for ^{12}C. Ultimately, this study suggests a link between the observed oceanographic perturbations (OD I) and the disappearance of *Saccocoma*-dominated microfacies.

ACKNOWLEDGEMENTS

The authors of this manuscript send the warmest thanks to István Főzy for his companionship during the field work, as well as his help in understanding of geology of the Transdanubian Range. The authors would also like to thank the journal reviewers and the editorial team for their constructive comments and efforts to improve the current paper. Last, but not least, the authors are also very grateful to Kristallina Stoykova for sharing the archival matrix of the nannofossil data from the Lókút succession. These investigations were financially supported by the National Science Center, Poland (project no.: 2016/21/B/ST/10/02941 leader: J. Grabowski; PGI-NRI, Warsaw) and OTKA/NKFI (project no: K135309; leader: J. Pálfy).

DATA AVAILABILITY STATEMENT

The data that support the findings of this study are available from the corresponding author upon reasonable request.

REFERENCES

Abbink, O., **Tarbarona, J.**, **Brinkhuis, H.** and **Visscher, H.** (2001) Late Jurassic to earliest Cretaceous palaeoclimatic evolution of the southern North Sea. *Glob. Planet. Chang.*, **30**, 231–256.

Algeo, T.J. and **Li, C.** (2020) Redox classification and calibration of redox thresholds in sedimentary systems. *Geochim. Cosmochim. Acta*, **287**, 8–26.

Algeo, T.J. and **Liu, J.** (2020) A re-assessment of elemental proxies for paleoredox analysis. *Chem. Geol.*, **540**, 119549.

Árgyelán, G.B. (1997) Ophiolitic detritus in the Lower Cretaceous sandstone of Gerecse Mountains, Hungary: petrography, detrital modes, provenance. *Miner. Slov.*, **29**, 262–263.

Bacelle, L. and **Bosselini, A.** (1965) Diagrammi per la stimavisiva della composizione percentuale nelle rocche sedimentarie. *Annali dell'Università di Ferrara*, **1**, 4.

Baumgartner, P.O. (2013) Mesozoic radiolarites – accumulation as a function of sea surface fertility on Tethyan margins and in ocean basins. *Sedimentology*, **60**, 292–318.

Baumgartner, P.O., **Li, X.**, **Matsuoka, A.** and **Vérard, C.** (2023) Austral and Subtropical Gyre Radiolaria – latest Jurassic to Early Cretaceous Leg 123, Site 765, Argo Abyssal Plain revisited: Southern Hemisphere paleobiogeography and global climate change. *Micropaleontology*, **69**, 555–633.

Błażejowski, B., **Pszczółkowski, A.**, **Grabowski, J.**, **Wierzbowski, H.**, **Deconinck, J.-F.**, **Olempska, E.**, **Teodorski, A.** and **Nawrocki, J.** (2023) Integrated stratigraphy and clay mineralogy of the Owadów-Brzezinki section (Lower–Upper Tithonian transition, Central Poland): implications for correlations between the Boreal and the Tethyan domains and palaeoclimate. *J. Geol. Soc. Lond.*, **180**, 1–17. https://doi.org/10.1144/jgs2022-073.

Bornemann, A., **Aschwer, U.** and **Mutterlose, J.** (2003) The impact of calcareous nannofossils on the pelagic carbonate accumulation across the Jurassic–Cretaceous boundary. *Palaeogeogr. Palaeoclimatol. Palaeoecol.*, **199**, 187–228.

Bover-Arnal, T. and **Strasser, A.** (2013) Relative sea-level change, climate, and sequence boundaries: insights from the Kimmeridgian to Berriasian platform carbonates of Mount Salève (E France). *Int. J. Earth Sci.*, **102**, 493–515.

Bown, P.R. and **Young, J.R.** (1998) Techniques. In: *Calcareous Nannofossil Biostratigraphy* (Ed Bown, P.R.), pp. 16–28. Chapman and Kluwer Academic, London.

Bureau Veritas Minerals Schedule of Service & Fees. (2020) https://commodities.bureauveritas.com/sites/g/files/zypfnx241/files/media/document/Metals%20Minerals%20and%20Environmental_2020_Fee_%20Schedule_MINING_CAD.pdf

Calvert, S.E. and **Pedersen, T.F.** (2007) Elemental proxies for palaeoclimatic and palaeoceanographic variability in marine sediments: interpretation and application. *Dev. Mar. Geol.*, **1**, 567–644.

Casellato, C.E. (2009) Causes and Consequences of Calcareous Nannoplankton Evolution in the Late Jurassic: Implications for Biogeochronology, Biocalcification and Ocean Chemistry. Ph.D. Thesis, Universita degli Studi di Milano, 122 p., Milano.

Casellato, C.E. (2010) Calcareous nannofossil biostratigraphy of Upper Callovian-Lower Berriasian successions from the Southern Alps, North Italy. *Riv. Ital. Paleontol. Stratigr.*, **116**, 357–404.

Casellato, C.E. and **Erba, E.** (2021) Reliability of calcareous nannofossil events in the Tithonian–early Berriasian time interval: implications for a revised high resolution zonation. *Cretac. Res.*, **117**, 104611.

Cecca, F., **Fourcade, E.** and **Azéma, J.** (1992) The disappearance of the "Ammonitico Rosso". *Palaeogeogr. Palaeoclimatol. Palaeoecol.*, **99**, 55–70.

Charbonnier, G., **Duchamp-Alphonse, S.**, **Adatte, T.**, **Föllmi, K.B.**, **Spangenberg, J.E.**, **Gardin, S.**, **Galbrun, B.** and **Colin, C.** (2016) Eccentricity paced monsoon-like system along the northwestern Tethyan margin during the Valanginian (Early Cretaceous): new insights from detrital and nutrient fluxes into the Vocontian Basin (SE France). *Palaeogeogr. Palaeoclimatol. Palaeoecol.*, **443**, 145–155.

Császár, G. and **Árgyelán, G.B.** (1994) Stratigraphic and micromineralogic investigations on Cretaceous Formations of the Gerecse Mountains, Hungary and their palaeogeographic implications. *Cretac. Res.*, **15**, 417–434.

De Wever, P., **O'Dogherty, L.** and **Goričan, Š.** (2014) Monsoon as a cause of radiolarite in the Tethyan realm. *Compt. Rendus Geosci.*, **346**, 287–297.

Deconinck, J.-F. (1993) Clay mineralogy of the late Tithonian–Berriasian deep sea carbonates of the Vocontian trough (SE France), relationship with sequence stratigraphy. *Bull. Centres Rech. Explor. Prod. Elf-Aquitaine*, **17**, 223–234.

Deconinck, J.-F., **Chamley, H.**, **Debrabant, P.** and **Colbeaux, J.P.** (1983) Le Boulonnais au Jurassique supérieur: données de la minéralogie des argiles et de la géochimie. *Ann. Soc. Géol. Nord*, **102**, 145–152.

Diester-Haass, L., **Robert, C.** and **Chamley, H.** (1993) Paleoceanographic and paleoclimatic evolution in the Weddell Sea (Antarctica) during the middle Eocene-late Oligocene, from a coarser sediment fraction and clay mineral data (ODP Site 689). *Mar. Geol.*, **114**, 233–250.

Erba, E. (1994) Nannofossils and superplumes: The early Aptian "nannoconid crisis". *Paleoceanography*, **9**, 483–501.

Erba, E. (2004) Calcareous Nannofossils and Mesozoic Oceanic Anoxic Events. *Mar. Micropaleontol.*, **52**, 85–106.

Erba, E., **Castradori, D.**, **Guasti, G.** and **Ripepe, M.** (1992) Calcareous nannofossils and Milankovitch cycles: the example of the Albian Gault Clay Formation (southern England). *Palaeogeogr. Palaeoclimatol. Palaeoecol.*, **93**, 47–69.

Fisher, R.A., **Corbet, A.S.** and **Williams, C.B.** (1943) The relation between the number of species and the number of individuals in a random sample of an animal population. *J. Anim. Ecol.*, **12**, 42–58.

Fodor, L., **Sztanó, O.** and **Kövér, S.** (2013) Mesozoic deformation of the northern Transdanubian Range (Gerecse and Vértes Hills). *Acta Mineralogica-Petrographica*, **31**, 1–52.

Főzy, I., **Janssen, N.M.M.**, **Price, G.D.**, **Knauer, J.** and **Pálfy, J.** (2010) Integrated isotope and biostratigraphy of a Lower Cretaceous section from the Bakony Mountains (Transdanubian Range, Hungary): a new Tethyan record of the Weissert event. *Cretac. Res.*, **31**, 525–545.

Gawlick, H.-J., **Missoni, S.**, **Schlagintweit, F.**, **Suzuki, H.**, **Frisch, W.**, **Krystyn, L.** and **Lein, R.** (2009) Jurassic tectonostratigraphy of the austroalpine domain. *J. Alpine Geol.*, **50**, 1–152.

Giraud, F., **Olivero, D.**, **Baudin, F.**, **Reboulet, S.**, **Pittet, B.** and **Proux, O.** (1998) Minor changes in surface-water fertility across the oceanic anoxic event 1d (latest Albian, SE France) evidenced by calcareous nannofossils. *Int. J. Earth Sci.*, **92**, 267–284.

Giraud, F., **Mattioli, E.**, **López-Otálvaro, G.**, **Lécuyer, C.**, **Suchéras-Marx, B.**, **Marineau, F.**, **Arnaud-Godet, F.** and **de Kænel, E.** (2016) Deciphering processes controlling mid-Jurassic coccolith turnover. *Mar. Micropaleontol.*, **125**, 36–50.

Grabowski, J., **Haas, J.**, **Márton, E.** and **Pszczółkowski, A.** (2010) Magneto- and biostratigraphy of the Jurassic/Cretaceous boundary in the Lókút section (Transdanubian Range, Hungary). *Stud. Geophys. Geod.*, **54**, 1–26.

Grabowski, J., **Haas, J.**, **Stoykova, K.**, **Wierzbowski, H.** and **Brański, P.** (2017) Environmental changes around the Jurassic/Cretaceous transition: new nannofossil, chemostratigraphic and stable isotope data from the Lókút section (Transdanubian Range, Hungary). *Sed. Geol.*, **360**, 54–72.

Grabowski, J., **Bakhmutov, V.**, **Kdýr, Š.**, **Krobicki, M.**, **Pruner, P.**, **Reháková, D.**, **Schnabl, P.**, **Stoykova, K.** and **Wierzbowski, H.** (2019) Integrated stratigraphy and palaeoenvironmental interpretation of the Upper Kimmeridgian to Lower Berriasian pelagic sequences of the Velykyi Kamianets section (Pieniny Klippen Belt, Ukraine). *Palaeogeogr. Palaeoclimatol. Palaeoecol.*, **532**, 109216.

Grabowski, J., **Chmielewski, A.**, **Ploch, I.**, **Rogov, M.**, **Smoleń, J.**, **Wójcik-Tabol, P.**, **Leszczyński, K.** and **Maj-Szeliga, K.** (2021a) Palaeoclimatic changes and inter-regional correlations in the Jurassic/Cretaceous boundary interval of the Polish Basin: portable XRF and magnetic susceptibility study. *Newsl. Stratigr.*, **54**, 123–158.

Grabowski, J., **Stoykova, K.**, **Wierzbowski, H.** and **Wójcik-Tabol, P.** (2021b) Upper Berriasian chemostratigraphy, clay minerals and calcareous nannofossils of the Barlya section (Western Balkan, Bulgaria): implications for paleoclimate and productivity changes, and stratigraphic correlations across the Alpine Tethys. *Palaeogeogr. Palaeoclimatol. Palaeoecol.*, **567**, 110252.

Grabowski, J., **Frau, C.**, **Schnabl, P.** and **Svobodová, A.** (2022) Magnetic susceptibility and gamma ray spectrometry in the Tré Maroua section (Tithonian/Berriasian, SE France) – terrigenous input and comparison with Tethyan record. *Volumina Jurassica*, **20**, 47–58.

Gröcke, D.R., **Price, G.D.**, **Ruffel, A.H.**, **Mutterlose, J.** and **Baraboshkin, E.** (2003) Isotopic evidence for Late Jurassic–Early Cretaceous climate change. *Palaeogeogr. Palaeoclimatol. Palaeoecol.*, **202**, 97–118.

Haas, J. and **Péró, C.** (2004) Mesozoic evolution of the Tisza Mega-unit. *Int. J. Earth Sci.*, **93**, 297–313.

Hallam, A., **Grose, J.A.** and **Ruffel, A.H.** (1991) Palaeoclimatic significance of changes in clay mineralogy across the Jurassic–Cretaceous boundary in England and France. *Palaeogeogr. Palaeoclimatol. Palaeoecol.*, **81**, 173–187.

Hesselbo, S.P., **Deconinck, J.-F.**, **Huggett, J.M.** and **Morgans-Bell, H.S.** (2009) Late Jurassic palaeoclimatic change from clay mineralogy and gamma-ray spectrometry of the Kimmeridge Clay, Dorset, UK. *J. Geol. Soc. Lond.*, **166**, 1123–1133.

Hesselbo, S.P., **Ogg, J.G.** and **Ruhl, M.** (2020) The Jurassic period. In: *Geologic Time Scale 2020* (Eds Gradstein, F.M., Ogg, J.G., Schmitz, M.D. and Ogg, G.M.), pp. 955–1021. Elsevier, Amsterdam, Oxford, Cambridge.with contributions by Hinnov, L.A. and Huang, C.J.

Hieronymus, B., **Kotschoubey, B.** and **Boulégue, J.** (2001) Gallium behaviour in some contrasting lateritic profiles from Cameroon and Brazil. *J. Geochem. Explor.*, **72**, 147–163.

Jach, R. and **Reháková, D.** (2019) Middle to Late Jurassic carbonate-biosiliceous sedimentation and palaeoenvironment in the Tethyan Fatricum domain, Krížna nappe, Tatra Mts, Western Carpathians. *Ann. Soc. Geol. Pol.*, **89**, 1–46.

Jenkyns, H.C., **Schouten-Huibers, L.**, **Schouten, S.** and **Sinninghe Damsté, J.S.** (2012) Warm Middle Jurassic–early Cretaceous high-latitude sea-surface temperatures from the Southern Ocean. *Clim. Past*, **8**, 215–226.

Jones, B. and **Manning, A.C.** (1994) Comparison of geochemical indices used for the interpretation of palaeoredox conditions in ancient mudstones. *Chem. Geol.*, **111**, 111–129.

Košťák, M., **Reháková, D.**, **Vaňkova, L.**, **Mazuch, M.**, **Trubač, J.** and **Milovský, R.** (2023) Slight carbon-isotope perturbation at the J/K boundary (base of the *Calpionella* Zone) – a proxy tool for correlation? A brief summary. *Cretac. Res.*, **151**, 105617.

Kozur, H. (1991) The evolution of the Meliata–Hallstatt ocean and its significance for the early evolution of the Eastern Alps and Western Carpathians. *Palaeogeogr. Palaeoclimatol. Palaeoecol.*, **87**, 109–135.

Kraus, M.J., **Woody, D.T.**, **Smith, J.J.** and **Dukic, V.** (2015) Alluvial response to Paleocene-Eocene thermal maximum climatic event, Polecat Bench, Wyoming (U.S.A.). *Palaeogeogr. Palaeoclimatol. Palaeoecol.*, **435**, 177–192.

Li, Y.-H. and **Schoonmaker, J.E.** (2003) Chemical Compositions and Mineralogy of Marine Sediments. *Treatise Geochem.*, **7**, 1–35.

Lodowski, D.G. and **Grabowski, J.** (2023) Tracing the latest Jurassic–earliest Cretaceous paleoenvironment evolution in carbonates: a case study of the Giewont succession (Central Western Carpathians, Poland). *Acta Geol. Pol.*, **73**, 741–772.

Lodowski, D.G., **Pszczółkowski, A.**, **Szives, O.**, **Főzy, I.** and **Grabowski, J.** (2022) Jurassic–Cretaceous transition in the Transdanubian Range (Hungary): integrated stratigraphy and paleomagnetic study of the Hárskút and Lókút sections. *Newsl. Stratigr.*, **55**, 99–135.

Mattioli, E., **Pittet, B.**, **Riquier, L.** and **Grossi, V.** (2014) The mid-Valanginian Weissert Event as recorded by calcareous nannoplankton in the Vocontian Basin. *Palaeogeogr. Palaeoclimatol. Palaeoecol.*, **414**, 472–485.

McLennan, S.M. (1993) Weathering and Global Denudation. *J. Geol.*, **101**, 295–303.

Michalík, J. (2007) Sedimentary rock record and microfacies indicators of the latest Triassic to mid-Cretaceous tensional development of the Zliechov Basin (Central Western Carpathians). *Geol. Carpath.*, **58**, 443–453.

Michalík, J., **Reháková, D.**, **Halásová, E.** and **Lintnerová, O.** (2009) The Brodno section – a potential regional stratotype of the Jurassic/Cretaceous boundary (Western Carpathians). *Geol. Carpath.*, **60**, 213–232.

Missoni, S. and **Gawlick, H.-J.** (2010) Jurassic mountain building and Mesozoic-Cenozoic geodynamic evolution of the Northern Calcareous Alps as proven in the Berchtesgaden Alps (Germany). *Facies*, **57**, 137–186.

Morales, C., **Gardin, S.**, **Schnyder, J.**, **Spangenberg, J.**, **Arnaud-Vanneau, A.**, **Arnaud, H.**, **Adatte, T.** and **Föllmi, K.B.** (2013) Berriasian and early Valanginian environmental change along a transect from the Jura Platform to the Vocontian Basin. *Sedimentology*, **60**, 36–63.

Nesbitt, H.W. and **Young, G.M.** (1982) Early Proterozoic climates and plate motions inferred from major element chemistry of litites. *Nature*, **299**, 715–717.

Niebuhr, B. (2005) Geochemistry and time-series analyses of orbitally forced Upper Cretaceous marl–limestone rhytmites (Lehrte West Syncline, northern Germany). *Geol. Mag.*, **142**, 31–55.

Pittet, B. and **Mattioli, E.** (2002) The carbonate signal and calcareous nannofossil distribution in an Upper Jurassic section (Balingen-Tieringen, Late Oxfordian, southern Germany). *Palaeogeogr. Palaeoclimatol. Palaeoecol.*, **179**, 71–96.

Price, G.D., **Főzy, I.** and **Pálfy, J.** (2016) Carbon cycle history through the Jurassic – Cretaceous boundary: a new global δ13C stack. *Palaeogeogr. Palaeoclimatol. Palaeoecol.*, **451**, 46–61.

Püttmann, T. and **Mutterlose, J.** (2021) Paleoecology of Late Cretaceous coccolithophores: insights from the shallow-marine record. *Paleoceanogr. Paleoclimatol.*, **36**, e2020PA004161.

Rameil, N. (2005) Carbonate sedimentology, sequence stratigraphy, and cyclostratigraphy of the Tithonian in the Swiss and French Jura Mountains. A high-resolution record of changes in sea level and climate. PhD thesis. *GeoFocus*, **13**, 246 pp.

Ratcliffe, K.T., **Wright, A.M.**, **Montgomery, P.**, **Palfrey, A.**, **Vonk, A.**, **Vermeulen, J.** and **Barrett, M.** (2010) Application of chemostratigraphy to the Mungaroo Formation, The Gorgon Field, offshore Northwest Australia. *APPEA J.*, **50**, 371–387.

Roth, P.H. (1984) Preservation of calcareous nannofossils and fine-grained carbonate particles in mid-Cretaceous sediments from the southern Angola Basin. In: *Initial Reports of the Deep Sea Drilling Project, 75*, pp. 651–655. U.S. Government Printing Office, Washingotn, D.C.

Rutsch, H.-J., **Mangini, A.**, **Bonani, G.**, **Dittrich-Hannen, B.**, **Kubik, P.W.**, **Suster, M.** and **Segl, M.** (1995) ^{10}Be and Ba concentrations in West African sediments trace productivity in the past. *Earth Planet. Sci. Lett.*, **133**, 129–143.

Schneider, R.R., **Price, B.**, **Müller, P.J.**, **Kroon, D.** and **Alexander, I.** (1997) Monsoon related variations in Zaire (Congo) sediment load and influence of fluvial silicate supply on marine productivity in the east equatorial Atlantic during the last 200,000 years. *Paleoceanography*, **12**, 463–481.

Schneider, A.C., **Heimhofer, U.**, **Heunisch, C.** and **Mutterlose, J.** (2018) From arid to humid – The Jurassic–Cretaceous boundary interval in northern Germany. *Rev. Paleobot. Palynol.*, **255**, 57–69.

Schneider, S., **Kelly, S.R.A.**, **Mutterlose, J.**, **Herrle, J.O.**, **Hülse, P.**, **Jolley, D.W.**, **Schröder-Adams, C.J.** and **Lopez-Mir, B.** (2020) Macrofauna and biostratigraphy of the Rollrock Section, northern Ellesmere Island, Canadian Arctic Islands – a comprehensive high latitude archive of the Jurassic–Cretaceous transition. *Cretac. Res.*, **114**, 104508.

Schnetger, B., **Brumsack, H.-J.**, **Schale, H.**, **Hinrichs, J.** and **Dittert, L.** (2000) Geochemical characteristics of deep-sea sediments from the Arabian Sea: a high-resolution study. *Deep-Sea Res. II*, **47**, 2735–2768.

Schnyder, J., **Gorin, G.**, **Soussi, M.**, **Baudin, F.** and **Deconinck, J.-F.** (2005) A record of the Jurassic/Cretaceous boundary climatic variation on the southern margin of the Tethys: clay minerals and palynofacies of the early Cretaceous Jebel Meloussi section (central Tunisia, Sidi Kralif Formation). *Bull. Soc. Geol. Fr.*, **176**, 171–182.

Schnyder, J., **Ruffel, A.**, **Deconinck, J.-F.** and **Baudin, F.** (2006) Conjuctive use of spectral gamma-ray logs and clay mineralogy in defining late Jurassic–early Cretaceous paleoclimate change (Dorset, U.K.). *Palaeogeogr. Palaeoclimatol. Palaeoecol.*, **229**, 303–320.

Schoepfer, S.D., **Shen, J.**, **Wei, H.**, **Tyson, R.V.**, **Ingall, E.** and **Algeo, T.J.** (2015) Total organic carbon, organic phosphorus, and biogenic barium fluxes as proxies for paleomarine productivity. *Earth Sci. Rev.*, **149**, 23–52.

Shen, J., **Schoepfer, S.D.**, **Feng, Q.**, **Zhou, L.**, **Yu, J.**, **Song, H.**, **Wei, H.** and **Algeo, T.J.** (2015) Marine productivity changes during the end-Permian crisis and Early Triassic recovery. *Earth-Sci. Rev.*, **149**, 136–162.

Szederkényi, T., **Haas, J.**, **Nagymarosy, A.** and **Hámor, G.** (2013) Geology and history of evolution of the ALCAPA mega-unit. In: *Geology of Hungary*, 244 pp (Ed Haas, J.). Springer, Heidelberg, New York, Dordrecht, London.

Szives, O. and **Főzy, I.** (2022) Towards the ammonite zonation of the Jurassic/Cretaceous transition: new data from ammonitico rosso/Biancone sections of the Transdanubian Range (Hungary). *Newsl. Stratigr.*, **55**, 385–426.

Tennant, J.P., **Mannion, P.D.**, **Upchurch, P.**, **Sutton, M.D.** and **Price, G.D.** (2016) Biotic and environmental dynamics through the Late Jurassic–Early Cretaceous transition: evidence for protracted faunal and ecological turnover. *Biol. Rev.*, **1**, 776–814.

Tian, J., **Xie, X.**, **Ma, W.**, **Jin, H.** and **Wang, P.** (2011) X-ray fluorescence core scanning records of chemical weathering and monsoon evolution over the past 5 Myr in the southern South China Sea. *Paleoceanography*, **26**, PA4202.

Tremolada, F., **Bornemann, A.**, **Bralower, T.J.**, **Koeberl, C.** and **van de Schootbrugge, B.** (2006) Paleoceanographic changes across the Jurassic/Cretaceous boundary: the calcareous phytoplankton response. *Earth Planet. Sci. Lett.*, **241**, 361–371.

Tribovillard, N., **Gorin, G.E.**, **Bielin, S.**, **Hopfgartner, G.** and **Pichon, R.** (1992) Organic-rich biolaminated facies from a Kimmeridgian lagoonal environment in the French Southern Jura mountains – a way of estimating accumulation rate variations. *Palaeogeogr. Palaeoclimatol. Palaeoecol.*, **99**, 163–177.

Tribovillard, N., **Algeo, T.J.**, **Lyons, T.** and **Riboulleau, A.** (2006) Trace metals as paleoredox and paleoproductivity proxies: an update. *Chem. Geol.*, **232**, 12–32.

Trujillo, A.P. and **Thurman, H.V.** (2011) *Essentials of Oceanography*, Tenth edn. 551 pp. Prentice Hall, Boston.

Turner, H.E. (2018) Integrated correlation of the Kimmeridge Clay Formation (Late Jurassic–early Cretaceous): a Boreal–Tethyan transect. PhD thesis. 212 p. School of Earth and Environmental Sciences, University of Portsmouth, UK.

Varol, O. and **Bowman, A.R.** (2019) Taxonomic revision of selected Late Jurassic (Tithonian) calcareous nannofossils and the application of mobile mounting. *Neues Jahrb. Geol. Palaontol. Abh.*, **291**, 65–87.

Vörös, A. and **Galácz, A.** (1998) Jurassic palaeogeography of the Transdanubian Central Range. *Riv. Ital. Paleontol. Stratigr.*, **104**, 69–83.

Vörös, A. and **Szives, O.** (2023) In between anoxic events: rise and fall of Pygopid brachiopods. (in Hungarian). 26. Magyar Őslénytani Vándorgyűlés, Abstract Volume and Field Trip Guide. pp. 37–38. Hungarian Geological Society, Budapest.

Vörös, A., **Főzy, I.** and **Szives, O.** (2019) Brachiopod distribution through the Jurassic–Cretaceous transition in the western Tethyan pelagic realm: Example from the Bakony Mountains, Hungary. *Cretac. Res.*, **104**, 104182.

Vörös, A., **Főzy, I.**, **Dulai, A.** and **Szives, O.** (2020) Late Valanginian extinction and turnover of Tethyan brachiopods: a signal of the Weissert Event (Bakony Mountains, Hungary). *Palaeogeogr. Palaeoclimatol. Palaeoecol.*, **555**, 109856.

Wei, G., **Li, X.-H.**, **Liu, Y.**, **Shao, L.** and **Liang, X.** (2006) Geochemical record of chemical weathering and monsoon climate change since the early Miocene in the South China. *Paleoceanography*, **21**, PA4214.

Weissert, H. and **Erba, E.** (2004) Volcanism, CO_2 and paleoclimate: a Late Jurassic – Early Cretaceous carbon and oxygen isotope record. *J. Geol. Soc. Lond.*, **161**, 1–8.

Weissert, H. and **Mohr, H.** (1996) Late Jurassic climate and its impact on carbon cycling. *Palaeogeogr. Palaeoclimatol. Palaeoecol.*, **122**, 27–43.

Weissert, H., **Lini, A.**, **Föllmi, K.B.** and **Kuhn, O.** (1998) Correlation of Early Cretaceous carbon isotope stratigraphy and platform drowning events: a possible link? *Palaeogeogr. Palaeoclimatol. Palaeoecol.*, **137**, 189–203.

Wignall, P.B. and **Ruffel, A.H.** (1990) The influence of a sudden climatic change on marine deposition in the Kimmeridgian of northwest Europe. *J. Geol. Soc. Lond.*, **147**, 365–371.

Wulf, L., **Mutterlose, J.** and **Bornemann, A.** (2020) Size variations and abundance patterns of calcareous nannofossils in mid Barremian black shales of the Boreal Realm (Lower Saxony Basin). *Mar. Micropaleontol.*, **156**, 101853.

Young, J.R., **Bown, P.R.** and **Lees, J.** (2017) *Nannotax3 Website*. International Nannoplankton Association, Birmingham, UK. http://www.mikrotax.org/Nannotax3.

Manuscript received 11 August 2023; revision accepted 24 March 2024

Supporting Information

Additional information may be found in the online version of this article:

Appendix S1 Most characteristic sedimentary features of the Hárskút (A) and Lókút (B) successions. Abbreviations: VAL. – Valanginian; murg. – Murgeanui; sim. – simplex; Mag. – Magnum; Fisch. – Fischeri; Praetin. – Praetintinnopsella. MF I – Saccocoma-

dominated microfacies; MF II – transitional microfacies; MF IIIA – calpionellid wackstone/packstone; MF IIIB – bioclastic wackestone/packstone. (A) Hárskút; (B) Lókút.

Appendix S2 Calcareous nannofossil and geochemical measurements database (.xlsx file).

Appendix S3 R-script file with statistical evaluation of calcareous nannofossil assemblages.

Appendix S4 Selected palaeoclimate proxies (Al/K, Ti/K, Th/K, CIA, Ga/Rb and Zr/Al) compared to variations in Al content in the Transdanubian Range sections.

Appendix S5 Selected palaeoredox proxies (authigenic U, EF U, Fe/Al and EF Mo) compared to variations in Al content in the Transdanubian Range sections.

Appendix S6 Variations in authigenic (biological) fraction content of selected micronutrient-type elements (P_{EXCESS}, Ba_{EXCESS}, Zn_{EXCESS} and $Cu_{EXCECSS}$) compared to variations in Al content in the Transdanubian Range sections.